NUMERICAL MODELING OF THE IMPACT OF PROJECTILES ON METAL STRUCTURES

Dragoljub M. Spasić

Serbian Armed Forces, General Staff, Directorate for Logistics (J-4),
Belgrade, Republic of Serbia,
e-mail: spasic.dragoljub@gmail.com,
ORCID iD: http://orcid.org/0000-0001-5570-955X

FIELD: Mechanical Engineering
ARTICLE TYPE: Review Paper
ARTICLE LANGUAGE: English

Summary:

This paper describes the numerical modeling of impact damage caused by impacts of projectiles on metal structures and the experimental results of impacts of projectiles of different shapes on metal structures. The experiments were carried out by the impact of projectiles on metal barriers of steel and aluminum of different thicknesses with the change in the impact speed of projectiles. In order to make the effects of experimental impact simulations as close as possible to real ones, the missile impacts are varied to match the average and limit speeds of impacts of projectiles that break obstacles. The obtained experimental results coincided well with the real effects on metallic obstacles and similar conducted tests from foreign literature.

Key words: aircraft, aircraft structure, impact, impact damage, modeling, missile, bullet projectile, penetrator, projectile penetration, penetration, ballistic protection.

Introduction

The impact of a projectile onto an obstacle at high speeds can cause various forms of damage to the obstacle. Depending on the speed of the projectile and the resistance of the obstacle, the projectile usually breaks through the obstacle, creates a surplus and / or stays in the obstacle or destroys the obstacle completely. The process that arises during the

impact of the projectile and its possible breakthrough is hard to conceive without any comprehensive experimental testing. However, numerical calculations in a combination with theoretical and experimental results provide a wide range of analyzes of different types of impacts from the point of view of materials used, geometry and variations of all parameters of the impact (initial projectile velocity, angle of impact).

Numerical modeling requires knowledge of both numerical methods and the mechanics of a rigid and deformable body (material resistance, theory of elasticity and plasticity, propagation of the deformation wave, etc.).

The earliest numerical simulations of impact and penetration were related to high impact and these early formulations did not include strength effects, so metals were treated as viscous fluids, and the terms "hydrodynamic computer codes" were used to refer to these computer programs (Anderson, 1987, pp.33-59). Anderson et al. (1994, pp.201-223) gave a brief history of the evolution and development of hydrocodes in relation to impact problems in which models of damage and deep penetration are particularly indicated. The most used models for determining possible structural damage in hydrosimulations required the definition of a critical value of voltage, deformation, plastic work, and other current criteria.

Penetration of high speed projectiles

In order to describe various phenomena that occur during ballistic penetration, it is necessary to characterize the behavior of materials in the conditions of impact load that generates high deformation rates. Characterization includes not only stress-deformation reactions in large deformations, different deformation rates and temperatures, but also the accumulation of damage and the type of damage. Such complex material behavior includes fractures which are difficult to describe with analytical models. In numerical simulations, constituent models of any degree of complexity can be incorporated into the code. However, although many difficulties in obtaining constants for dynamic material behavior are present, engineering models are preferred for more sophisticated models. The first problem examined is the penetration of an aluminum plate with a projectile made of Arne tool steel and the second problem is the penetration of a steel target with a projectile made of Arne tool steel as well (Backman & Goldsmith, 1978, pp.1-99).

Low density, high specific strength, good energy absorption, good corrosion resistance, good thermal conductivity and poorer sensitivity to adiabatic shear and thermoplastic instability are the characteristics of aluminum alloys that make them suitable for this purpose. In addition, many aluminum alloys can easily be shaped into complex structures.

In this paper, the perforation of a Weldox 460E steel plate and an aluminum plate with a steel projectile will be considered. The most important characteristic that points to the protective capability and resistance of the impact board is the ballistic limit i.e. ballistic boundary velocity which represents the greatest speed of impact of the projectile in which the plate will not break. In order to determine the ballistic speed and the remaining speed in the past, analytical and empirical models were created; they could somehow predict the behavior of the materials exposed to impact. With the development of computer technology, a possibility of numerically solving this problem was created. The most commonly used methods for numerical stroke calculation are the Finite Element Method (FEM) and the Smooth Particle Method (SPH). Lately, a combination of these two methods, the SFM method, has become increasingly popular.. In this paper, we will show the analysis of the impact of a projectile with a sharp tip on a flat aluminum plate and compare the results obtained with the FEM and SFM methods with the experimental results.

Constitutional model

The impact is often caused by the plastic flow of materials with high deformation rates, local temperature rise and material cracking. The standard approach to solving the problem of impact involves two different constituent models: one that defines plasticity and the other that defines the criterion of damage (breakdown) of the material. In the literature for this type of analysis, Jonson-Kukow (JS) constitutive models are most often used, and for this reason they will be used in this paper as well. These two models are not linked and can be used separately.

Johnson & Cook created a constitutive model for metals exposed to large deformations, high deformation rates and high temperatures, primarily designed for impact calculations (Johnson & Cook, 1985, pp.31-48). In order to define the characteristics of the material, this model uses five different coefficients which must be determined by experimental testing. Johnson & Cook presented Fon Mises's flow stress with the relation:

$$\bar{\sigma} = \left[A + B \dot{\bar{\varepsilon}}_p^n \right] \left[1 + C \ln \dot{\bar{\varepsilon}}_p^* \right] \left[1 - T^{*m} \right] \tag{1.1}$$

where $\bar{\sigma}$ is the von Mises equivalent of voltage. The coefficients A, B, n, C and m are the material constants. The constant A is the flow stress, B and n are the results of hardening, and C is the deformation rate constant. $\dot{\bar{\varepsilon}}_p^* = \dot{\bar{\varepsilon}}_p / \dot{\varepsilon}_0$ is the dimensionless deformation speed, $\dot{\bar{\varepsilon}}_p$ is the the quivalent plastic deformation, $\dot{\varepsilon}_0$ is the reference deformation rate,

T^* is the corresponding homogeneous temperature defined as $T^* = (T - T_r)/(T_m - T_r)$, and T is the absolute temperature, while the exponents *r* and *m* indicate the room temperature and the melting temperature. Borvik et al (2003, pp.413-464), (2004, pp.367-384) made the modification of Johnson-Kook's model and his relation is in the form:

$$\overline{\sigma} = \left[A + B\overline{\varepsilon}_p^n\right]\left[1 + \dot{\overline{\varepsilon}}_p^*\right]^C\left[1 - T^{*m}\right]$$ (1.2)

In this model, we can see that when the deformation rates are approximate, i.e. uniform, then the deformation rate tends to zero, which has a great advantage in determining the model parameters and for the numerical implementation of this model.

By combining an elasto-high-plastic model with ductile damage, a quasi-Fon Mises voltage is given as

$$\overline{\sigma} = \left[1 - \beta D\right]\left[A + Br^n\right]\left[1 - \dot{r}^*\right]^C\left[1 - T^{*m}\right],$$ (1.3)

where *D* is variable damage, taking the values between 0 as conditional and 1, when a complete breakthrough occurs, $\dot{r} = (1 - \beta D)$ is the damage equivalent to the plastic deformation rate, and $\dot{r}^* = \dot{r}/\dot{\varepsilon}_0$ is the dimensional damage equivalent to the plastic deformation rate.

Lee & Yoo (2001, pp.819-829) have also taken into account the effect of temperature increase resulting from the adiabatic heating of materials, i.e. work that transforms into heat when it flows into heat:

$$\dot{T} = x\frac{\overline{\sigma}\varepsilon_p}{\rho C_p},$$ (1.4)

where ρ is density, C_p is specific heat, and *x* (Taylor, 1948, pp.103-124) is the empirical coefficient which represents a ratio which transforms into heat in a plastic flow. For metal plates, it is usually assumed that this coefficient is 0.9.

The authors of this paper consider that satisfactory results can be obtained by the original Johnson-Kuk model, and for this reason only the standard unconfigured Johnson-Kuk's constitutive model of material strength will be used. As a criterion for material fracture, Johnson & Cook proposed a constituent model adapted to computer simulations, and it is represented by relations:

$$\sigma = \left[A + B(\varepsilon_p)^{\mu}\right]\left[1 + C\ln\dot{\varepsilon}_{eff}\right]\left[1 - \left(\frac{(T - T_r)}{(T_m - T_r)}\right)^b\right]$$ (1.5)

$$D = \sum_{t=0}^{t_C} \frac{\Delta\varepsilon}{\varepsilon^f} \qquad (1.6)$$

$$\varepsilon^f = \left[D_1 + D_2 \exp D_3\left(\frac{\sigma_a}{\sigma_e}\right) \right]\left[1 + D_4 \ln \dot{\varepsilon}_{eff}\right]\left[1 - D_S T^*\right], \qquad (1.7)$$

where ε^f is the equivalent deformation to fracture under the current temperature conditions, $(\varepsilon_0=1s-1)$ and ε_p are equivalent and plastic stretching, $\dot{\varepsilon}_{eff} = \varepsilon_p / \varepsilon_0$ the effective stretching rate, T_m and T_r are the reference flow temperature and room temperature, tc is the time in the time of impact, σ_a and σ_e are average normal and equivalent voltage and *A*, *B*, *a*, *C* and b are the constants of the material.

In these relations, *D* represents five parameters of the element damage and a fracture is possible when *D=1*.

Modeling of materials

Johnson-Cook's constituent models of strength and breakage of materials were used for the numerical analysis in this paper. The material used in the analyses is a Weldox 460E steel plate and an aluminum alloy AA5083-H116 plate. This alloy belongs to the class AA5xxx, i.e. aluminum-magnesium alloys. It has good rolling properties and is therefore convenient for use; it also has good corrosion resistance. The AA5083-H116 alloy is the second-strongest commercial aluminum-megane-based alloy. A detailed analysis of the material characteristics and the definition of the coefficients for Johnson-Kuk's constitutive models were done by Clausen et al. (2004, pp.260-272).

The characteristics of the materials and the values of the coefficients used in the analyses are shown in Tables 1-3.

Table 1 – Characteristics of the materials for the Weldox460E steel plate
Таблица 1 – Характеристики материалов для стальной плиты Weldox460E
Табела 1 – Карактеристике материјала за челичну плочу Weldox460E

E [GPa]	V	ρ [kg/m3]	A [MPa]	B [MPa]	$\dot{\varepsilon}$ [s-1]	n	C	m	Dc
200	0.33	7850	490	807	1	0.73	0.00114	0.94	0,30
Cp [J/kgK]	α	$\overline{\alpha}$ [K-1]	Tt [K]	Ta [K]	D1	D2	D3	D4	D5
910	0.9	1.1×10^{-5}	1800	293	0.0705	1.732	-0.54	-0.015	0

Table 2 – Characteristics and constants for the AA5083-H116
Таблица 2 – Характеристики и константы AA5083-H116
Табела 2 – Карактеристике и константе за AA5083-H116

E [GPa]	ν	ρ [kg/m3]	A [MPa]	B [MPa]	$\dot{\varepsilon}$ [s-1]	n	C	m	Dc
70	0.3	2700	167	596	1	0.551	0.001	0.859	1
Cp [J/kgK]	α	$\overline{\alpha}$ [K-1]	Tm [K]	T0 [K]	D1	D2	D3	D4	D5
452	0.9	2.3 x 10^{-5}	893	293	0.0261	0.263	-0.349	0.147	16.8

The projectile is modeled with the characteristics of Arne tool steel. Its characteristics are shown in Table 3.

Table 3 – Characteristics of Arne tool steel
Таблица 3 – Характеристики инструментальной стали Арне
Табела 3 – Карактеристике алатног челика арне

σ_Y [GPa]	ν	ρ [kg/m3]	E [GPa]	Et [MPa]	ε_t [%]
1.9	0.33	7850	204	15	2.15

In this study, steel projectiles with different tip shapes and dimensions (blunt, conical and hemispherical) were used to simulate perforation and penetration (piercing, deep damage and blooming) of steel and aluminum plates.

(I) The blunt projectile was used to test impact damage including the perforation of the Weldox 460E steel plate with a plate thickness of 6, 8, 10, 12, 16 and 20 mm,

(II) Perforation of steel plates with a thickness of 12 mm projectiles of different tips, and

(III) Perforation of AA5083-H116 aluminum plates with conical steel projectiles with thicknesses of 15, 20, 25 and 30 mm.

The simulated values of initial velocities and ballistic boundary velocities are compared with the experimental results.

In high-speed impacts, materials are usually subjected to extreme stretching, high impact of plastic deformations, increased temperature and serious damage. The constitutive bond for metals, Johnson-Kook's model, was proposed considering all the above parameters, Johnson-Kuk's model materials. The damage parameter, stretching and fracture are expressed in the original form, as in the equations from 1.5 to 1.7.

Numerical analysis

Independently of the experimental testing, the mechanisms of damage to the steel Weldox 460E plates and the AA5083-H116 aluminum plates during a ballistic shock can be determined using numerical simulations. Although this

method has become popular in characterizing all types of materials,it has to be used with caution and always confirmed by experiments. It is also uncertain whether experimental testing can be completely replaced by a numerical simulation.

A numerical simulation of the problem of impact on the steel and aluminum plates was carried out by a projectile from Arne tool steel and analyzed to obtain estimates of global damage. All these predictions were made using the numerical code of the final difference of the AUTODYN-2D and 3D program, and then compared with the experimental data to illustrate the simulation performance. Autodyn has seven different solverers for spatial discretization: Lagrange, Shellm, Beam, ALE, SPH, Euler-FCT, and Euler-Godunov. When it comes to balistics problems, the most commonly used ones are the Lagrange and SPH solvers. The SPH is also a Lagrange method based on the interaction of adjacent particles.

Numerical calculations have been made for the Weldox 460E steel and AA5083H116 aluminum sheets of different thicknesses and different initial projectile speeds. The geometry of the projectiles and the shapes of the tips are shown in Figure 1.

Software for explicit solving of the equations of the state in the Langranges coordinates was used for numerical calculations. The Lagrange formulation is easier to apply for this type of calculations, because with the Euler formulation, there are difficulties in precisely defining deformable material boundaries and the contact between the projectiles and the plates. In the Lagrange formulation, the net moves and deforms with the material which is modeled so that the maintenance of the mass is automatically satisfied. If we consider the three-dimensional (3D) body occupied by the Lagrange space of the volume V undergoing the` stretch $f_{ti}(t)$ over the part of the external surface of S_t and with the force of the external body $f_{bi}(t)$, we obtain that the virtual work is equal to:

$$\int_V \rho \ddot{u}_{ui} \delta u_i dV + \int_V \sigma_{ij} \delta u_{i,j} dV - \int_V \rho f_{bi} \delta u_i dV - \int_{s_t} f_{ti} \delta u_i ds = 0 \qquad (1.8)$$

where ρ is the density of the material, σ_{ij} the Kosi stress tensor, $u_{i,j}$ acceleration, and δu_u necessary virtual displacement.

By applying spatial discretization to the finite elements of equation 1.8, the main equation becomes:

$$[M](\ddot{u}) + [K](u) = (F) \qquad (1.9)$$

$$[M] = \sum_{n_1=0}^{n_{total}} \int_V \rho [N]^t [N] dV_e \qquad (1.10)$$

where the *M*, *K* and *N* matrices are a function of mass, stiffness and shape, n_{total} is the total number of elements in the domain, V_e is the volume of the element, and *F* is the equivalent vector of the nodal force of the combined internal and external forces, including those obtained by restoring the body during the impact. For the problem of high velocity impact, the method of explicit central difference in time for solving equation 1.10 is used.
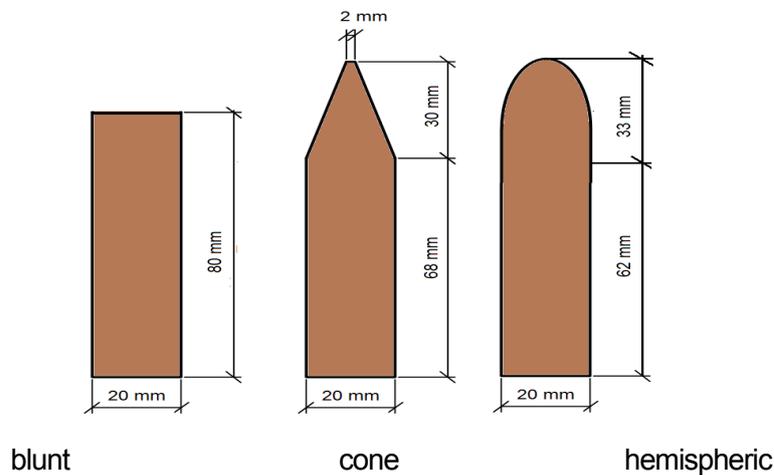
Figure 1 – Geometry and dimensions of projectiles with different tip shapes
Рис. 1 – Геометрические формы и размеры снарядов с различными головками
Слика 1 – Геометрија и димензије пројектила са различитим облицима врхова

The Smooth Particle Hydrodynamics Method (SPH) is a non-homogeneous Lagrange method which can naturally solve problems involving large deformations and serious material damage, and is therefore a convenient tool for solving high-speed impact problems. The method was first developed by (Lucy, 1977, pp.1013-1024), (Gingold & Monaghan, 1977, pp.375-389) to describe astrophysical phenomena. The system is represented by a set of particles, and the variable to the observed domain is calculated using the use of interpolation functions. An integral representation or approximation of the core function *f(x)* by an overlapping subdomain of the influence *Ω* can be expressed as:

$$\{f(x)\} = \int_\Omega f(x_i) W(x - x_i, h) dx_i \qquad (1.11)$$

where W is the core alignment function, and h is the alignment length that represents the unit measure of the subdomain of the effect of the function *W* (Figure 2a). To satisfy the required partition of the unit condition, the interpolation function must be normalized in each subdomain:

$$\int_{\Omega} f(x_i)W(x - x_i, h)dx_i = 1 \tag{1.12}$$

The commonly used interpolation function, the cubic "B-spline", is expressed as:

$$W_{(q,h)} = \frac{K}{h^{\xi}}\begin{cases} 1 - \left(\frac{3}{2}\right)q^2 + \left(\frac{3}{4}\right)q^3 & q \le 1 \\ \left(\frac{1}{2}\right)(2 - q)^3 & 1 < q \le 2 \\ 0 & q > 2 \end{cases} \tag{1.13}$$

where *q=(x-xi)/h, (ξ=1,2 or 3)* is the dimension of the problem, and *K* is the scaling factor for agreement with equation 5.12.
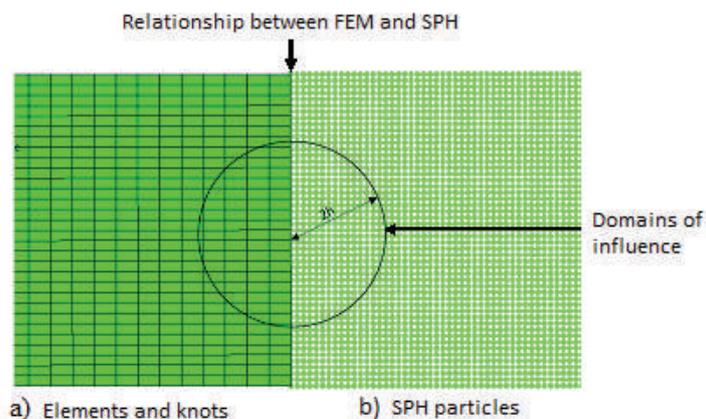
Figure 2 – Coupled SPH and FEM methods
Рис. 2 – Сопряженный SPH и FEM метод
Слика 2 – Спрегнута СПХ и ФЕМ метода

Based on the conservation of mass, moment and energy in the solid-state mechanics, the SPH basic equations express the causal differential equations of maintaining the amount of motion that connect the acceleration to the voltage tensor and look like:

$$\rho\ddot{x} = b_x + \frac{\partial \sigma_{xx}}{\partial x} + \frac{\partial \sigma_{xy}}{\partial y} + \frac{\partial \sigma_{xz}}{\partial z} \qquad (1.14)$$

$$\rho\ddot{y} = b_y + \frac{\partial \sigma_{yx}}{\partial x} + \frac{\partial \sigma_{yy}}{\partial y} + \frac{\partial \sigma_{yz}}{\partial z} \qquad (1.15)$$

$$\rho\ddot{z} = b_z + \frac{\partial \sigma_{zx}}{\partial x} + \frac{\partial \sigma_{zy}}{\partial y} + \frac{\partial \sigma_{zz}}{\partial z}, \qquad (1.16)$$

where ρ, σ and b are density, voltage and acceleration in the direction of the axes x, y and z in the original form.

The energy conservation equation is represented by the relation:

$$\dot{e} = \frac{1}{\rho}(\sigma_{xx}\dot{\varepsilon}_{xx} + \sigma_{yy}\dot{\varepsilon}_{yy} + \sigma_{zz}\dot{\varepsilon}_{zz} + 2\sigma_{xy}\dot{\varepsilon}_{xy} + 2\sigma_{yz}\dot{\varepsilon}_{yz} + 2\sigma_{zx}\dot{\varepsilon}_{zx}) \qquad (1.17)$$

It should be noted that explicit software only imposes the conservation of mass and quantity of motion, while the conservation of energy is observed due to the evaluation of the quality of the solution. The lack of solving Lagrange's formulation by the finite element method is the problem of large distortion of elements, interruption of elements and the occurrence of negative volumes. There are methods for solving this problem, for example by introducing elements erosion; however, more recent introduction of the SPH domains in the domain of large deformations is becoming more and more important. The SPH is a non-homogeneous Lagrange method developed to describe astrophysical phenomena; however, it is suitable for solving the problem of impacts in which major deformations and material damage are present. With the SPH method, the system is represented by a set of particles and their variables are counted using the Kernel interpolation function. The integral representation, i.e. the kernel approximation for the function f(x) for the subdomain Ω is presented in the form:

$$\langle f(x) \rangle \cong f(x')W(x - x', h)dx' \qquad (1.18)$$

where W is the Kernel function, and h is the domain effect influence of the W function. The Cuban B-spline function is most often used to align the Kernel function. The combined (matched) method (SFM) is used for the optimization and the best use of computer programs. This method models the SPH domain only in the domain of large deformations, i.e. where large damage is expected, which reduces the number of SPH particles and, therefore, significantly reduces time for calculations. The use of the FEM for the rest of the calculation domain improves the accuracy of the solution. The SPH

particles with the domain of influence and the SPH-FEM interface in the SFM method are shown graphically in Figure 2.

For numerical testing, the SFM simulations of the perforations of the Weldox 460E steel and AA5083-H116 aluminum plates of variable thicknesses were performed by projectiles of various tips (blunt, conical and hemispherical). The geometry of three projectiles of different tip shapes is shown in Figure 1 (Anderson, 2005, pp.135-142).

The modeling of each individual target plate consists of two regions. For all analyzes, both for the method of finite elements and for the combined method, an axisymmetric model was used. The parts of the FEM and SFM networks used for the analysis are shown in Figure 3, for conical, blunt and hemispherical projectiles. Numerical SPH particles are adopted in the vicinity of impacts where damage and large deformations are expected, while the rest of the target domain and projectiles are modeled using the use of finite elements as shown in Figure 3. The problem can be reduced to an axially symmetrical flat case or a spatial one when a quarter of the domain is modeled, given the symmetry in the x_3 and y_3 planes, where the boundary conditions of the symmetry are imposed on the FEM network. The set of particles is defined to provide the symmetry condition for the SPH region.
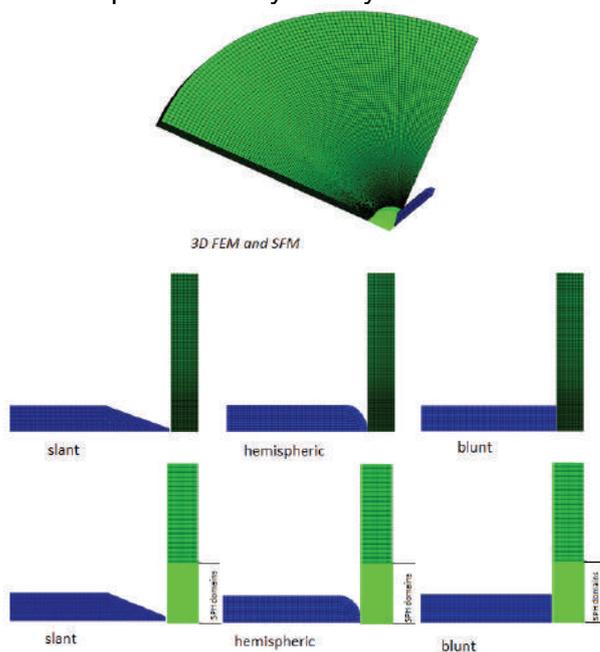
Figure 3 – 3D and 2D FEM and SFM projector networks and projectiles
Рис. 3 – 3Д и 2Д FEM и SFM расчетная модель траектории снаряда
Слика 3 – Прорачунске мреже плоче и пројектила 3D и 2D ФЕМ и СФМ

73

The numerical simulations performed in this paper were carried out using the Autodyn software, 2D and 3D for two-dimensional and three-dimensional problems, respectively. This program is based on finite difference methods, finite volumes and finite elements. It also possesses the possibility of calculating with the so-called meshless method, ie. by the method of hydrodynamics of smooth particles, which is suitable for calculations where large deformations and high deformation rates occur, as in this case. If one of the above mentioned networks is used, it is necessary to take into account the erosion of the elements.

The Johnson-Kook material model was adopted for target plates, while each projectile was modeled as a simple elastic-plastic material with isotropic hardening. The important constants of materials for steel and aluminum specific plates and solidified steel projectiles are given in Tables 1-3.

Analysis of the influence of different input parameters on the results of numerical calculations

The initial numerical results of the perforation of the steel plate by cone projectiles using the SFM show that natural speeds are sensitive to the distance of SPH particles. The network sensitivity phenomenon is also observed for the FEM simulation by Dey (Dey, 2004) who considers it to be a consequence of a localized adiabatic projection in the area around the penetration of the projectile. Therefore, the study was carried out to investigate the effects of SPH particle distances for two samples: Weldox 460E steel plates with a thickness of 12 mm and aluminum plates with a thickness of 15 mm. The SPH convergence study for two cases, as shown in Figure 4, shows that reasonable convergence results can be achieved using the distance of the SPH particles of 0.6 mm, which is the value adopted for the subsequent calculations. The SPH distance effects were tested for projectiles with a sharp conical tip as well and the results confirmed that the same 0.6 mm particle distance can be adopted.

The melting temperature and the strength of the plates used for testing affect the friction coefficient values used in this study. The lower melting temperatures tend to produce a thinner layer between the plate (target) and the projectile, which acts as a lubricant. In the published paper, photomicrography of the penetration of an aluminum target plate with a spherical top projectile at an initial velocity of 120 [m/s] shows significant microstroutural changes in a thin layer of 5 - 15 µm in a plane around the projectile (Rosenberg & Yeshurun, 1988, pp.357-362), (Rosenberg & Tsaliah, 1990, pp.247-251). A similar behavior is observed for other sharp-pointed missiles, such as conic and pointed tips, on the contact surface between the target material (target) and the projectile, when the target moves vertically. Such an event tells us that sliding

friction between projectiles and targets exists and must be taken into account. The mentioned layer was not perceived for the perforation of a blunt projectile, because the target plate was broken due to localized adiabatic shear, causing negligible contact friction between the projectile and the target. This was confirmed by the perceived constant natural velocity after damaging the plate due to the adiabatic shear of "splitting" and compacting the blunt projectile, which (Borvik et al, 2003, pp.413-464), (Borvik et al, 2004, pp.367-384) published in his scientific papers.
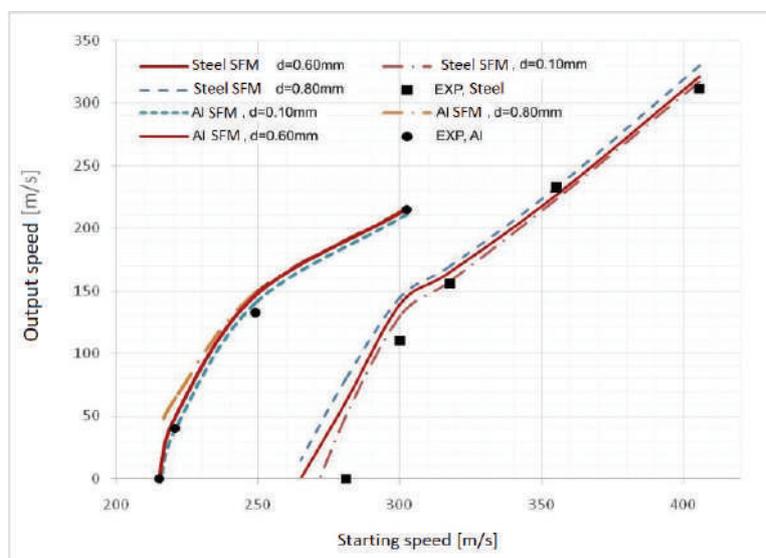
Figure 4 – An analysis of the distances of SPH particles for the impact of the conical projectile on the steel plate of 12 mm and the aluminum plate of 15 mm
Рис. 4 – Анализ расстояния SPH частиц от удара остроконечного снаряда о стальную плиту 12 мм и алюминиевую плиту 15 мм
Слика 4 – Анализа удаљености СПХ честица за удар конусног пројектила о челичну плочу дебљине 12 mm и алуминијумску плочу дебљине 15 mm

Choosing the appropriate friction coefficient value, µ, is complex because no experimental data is currently available for high velocity. Ravid & Bodner (1983, pp.577-591) presume the values of *µ = 0.1* and *µ = 0.05* for the perforation of steel plates by high-velocity missiles for the frontal and lateral surface of the projectile. A lower value for the lateral surface of the projectile is expected due to the high velocity effect and the presence of a thin viscous film, as the material temperature increases over the melting point in the contact surface. In order to compare the data from this paper, tests with three different friction coefficient values were carried out, for µ from 0.0, 0.05 and 0.1, which were used for perforations with a conical tip projectile through a steel target

plate of 12 mm thickness. The natural display versus the initial velocity of the projectile with the adopted three values *μ* are given in Figure 24. A significant effect of friction at a natural velocity can be noticed. The friction coefficient *μ = 0.05* indicates that it provides a reasonably accurate result simulated over the SFM. In the following simulations, perforation with conical tip projectiles was adopted. Also, in further analyzes, a simulation was performed for blunt missiles with the friction coefficient *μ = 0.02* for different thicknesses of steel plates (6, 8, 10, 12 and 16 mm) and at different speeds, but only for the FEM method. The simulations are shown in Figures 29 through 34. In the analysis of the SFM method, it is noted that with the influence of friction, the erosion of the elements at the exit of the projectile occurs, so that they are not considered with the influence of friction (Spasić, 2015).

In order to compare the data from the studied scientific papers, the experimental data were compared with those derived from the friction coefficient μ of 0.0, 0.05 and 0.1 for a 15 mm thick AA5083.H116 aluminum plate perforated with a conical tip projectile. Figure 5 shows the numerical results used for the indicated values, where it is also confirmed that the results agree well with the results of the impact test. This value was adopted for the subsequent analysis of the aluminum plate perforation.
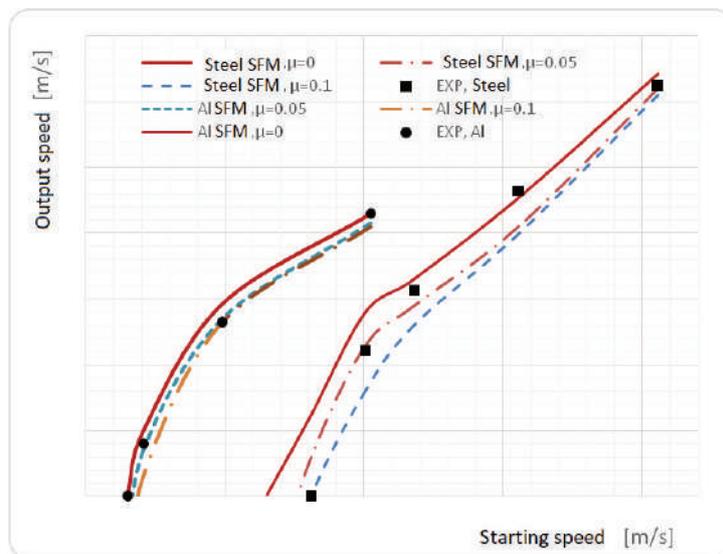
Figure 5 – Friction effects in the perforation of a 12 mm thick steel plate and s 15 mm aluminum panel by conical projectiles
Рис. 5 – Эффекты трения при перфорации стальной плиты, толщиной 12 мм и алюминиевой плиты, толщиной 15 мм, остроконечным снарядом
Слика 5 – Ефекти трења при перфорацији челичне плоче дебљине 12 mm и алуминијумске плоче дебљине 15 mm конусним пројектилом

Analysis of weldox 460e steel plate perforation
Perforation of blunt projectiles by the SFM method

In this part, an analysis of the perforation of steel plates of different thicknesses of 6, 8, 10, 12, 16 and 20 mm was performed, due to different speeds with a blunt projectile, using the 2D SFM method of Autodyn. Numerical natural and ballistic boundary speeds are compared with the experimental data published by (Borvik et al, 2003, pp.413-464), (Borvik et al, 2004, pp.367-384) in his work. In the paper, it has been confirmed that, except for thin plates, at relatively low initial velocities of the projectile of about 170 [m/s] and less, the SFM results agree well with the experimental values. Figures 6 to 11 show the results of a numerical analysis of blunt projectiles at various speeds of 435.6 [m/s] to 145 [m/s] for plates of 6, 8, 10, 12, 16 and 20 mm thicknesses.
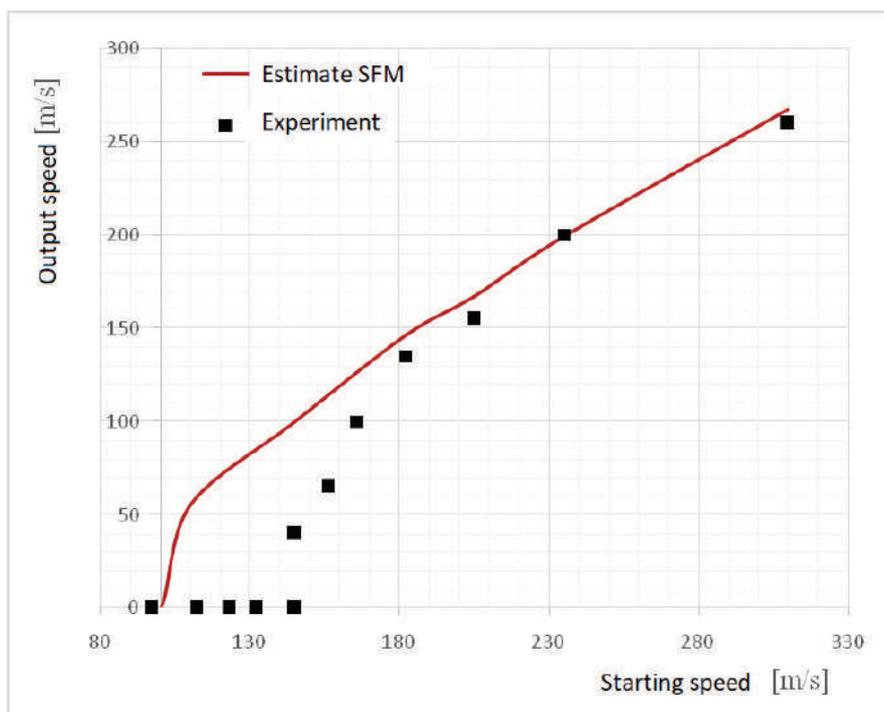
Figure 6 – Analysis of the SFM by a blunt projectile for a plate with a thickness of 6mm
Рис. 6 – Анализ SFM тупоконечным снарядом на плиту, толщиной 6 мм
Слика 6 – Анализа СФМ тупим пројектилом за плочу дебљине 6 тт
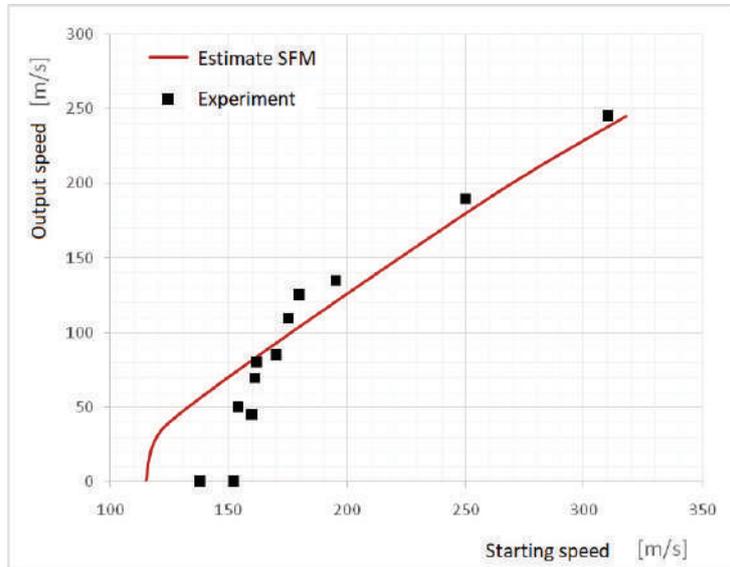
Figure 7 – Analysis of the SFM by a blunt projectile for a plate with a thickness of 8 mm
Рис. 7 – Анализ SFM тупоконечным снарядом на плиту, толщиной 8 мм
Слика 7 – Анализа СФМ тупим пројектилом за плочу дебљине 8 mm
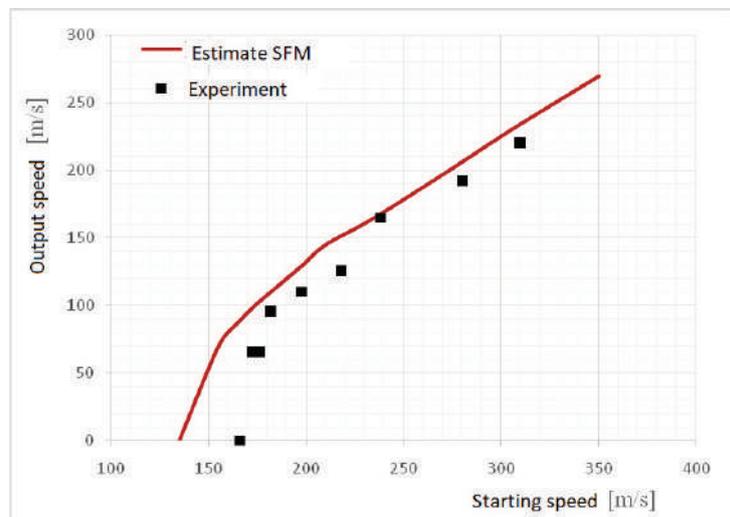
Figure 8 – Analysis of the SFM by a blunt projectile for a plate with a thickness of 10 mm
Рис. 8 – Анализ SFM тупоконечным снарядом на плиту, толщиной 10 мм
Слика 8 – Анализа СФМ тупим пројектилом за плочу дебљине 10 mm
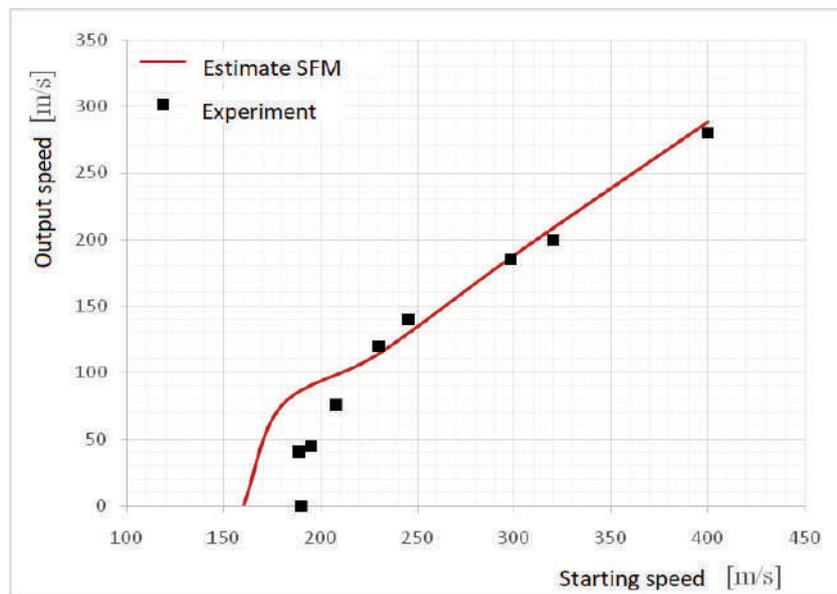
Figure 9 – Analysis of the SFM by a blunt projectile for a plate with a thickness of 12 mm
Рис. 9 – Анализ SFM тупоконечным снарядом на плиту, толщиной 12 мм
Слика 9 – Анализа СФМ тупим пројектилом за плочу дебљине 12 mm
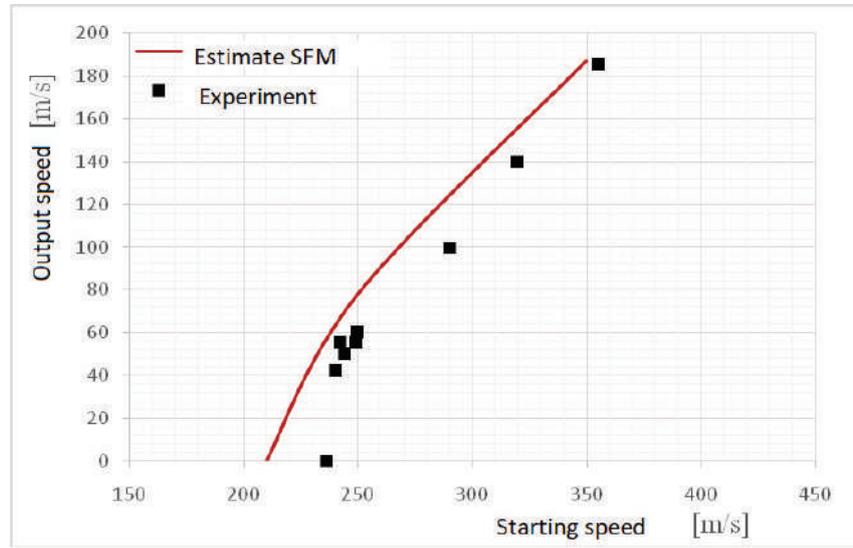
Figure 10 – Analysis of the SFM by a blunt projectile for a plate with a thickness of 16 mm
Рис. 10 – Анализ SFM тупоконечным снарядом на плиту, толщиной 16 мм
*Слика 10 – Анализа СФМ тупим пројектилом за плочу дебљине 16 mm*
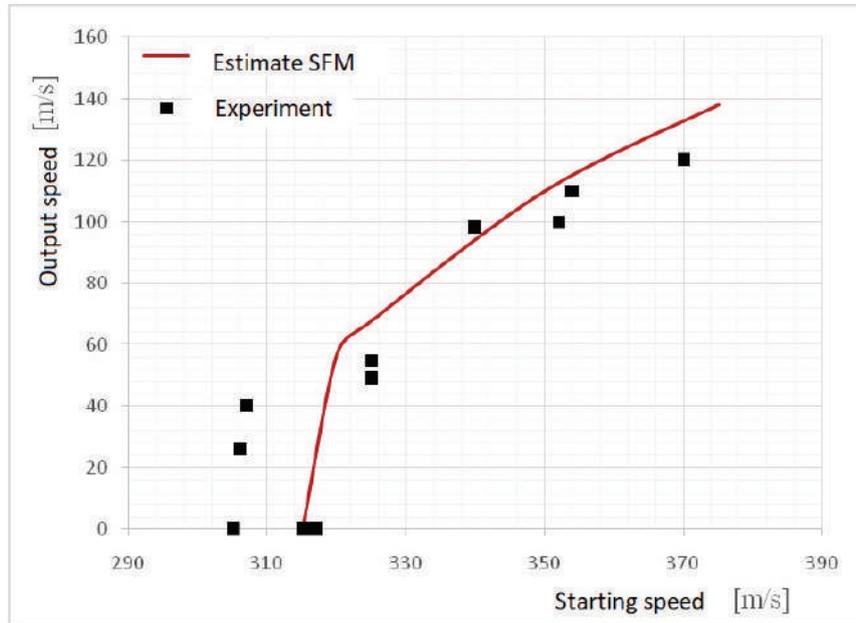
Figure 11 – Analysis of the SFM by a blunt projectile for a plate with a thickness of 20 mm
Рис. 11 – Анализ SFM тупоконечным снарядом на плиту, толщиной 20 мм
Слика 11 – Анализа СФМ тупим пројектилом за плочу дебљине 20 mm

Ballistic limit speed is defined as the minimum projectile speed required to break the target plate. The obtained results indicate that the application of the SFM method for blunt missiles, especially for thin slabs of 10 mm and lower values of ballistic boundary velocities, deviates from the experimental results, as well as in the results published by (Borvik et al, 2003, pp.413-464), (Borvik et al, 2004, pp.367-384). This slope difference is explained as a change in the shape of a fracture of adiabatic shear and fracture by compression for thick slabs to global propagation and thin panel slab fracture.

Perforation of blunt projectiles by the FEM method

For the comparison of the obtained results, the analysis of the perforation of steel plates with different thicknesses of 6, 8, 10, 12, 16 and 20 mm was performed, due to different speeds with a blunt projectile using the 2D FEM method for the Autodyn program. In this analysis, using the FEM method for all plate thicknesses, an analysis was performed using the friction effect $\mu = 0.02$. The analysis was performed for a range of speeds of 145.3 [m/s] to 435.6 [m/s]. The results for boundary ballistic and natural velocities for plates of various thicknesses from 6 mm to 20 mm are shown in the diagrams in Figures 12 to 17.
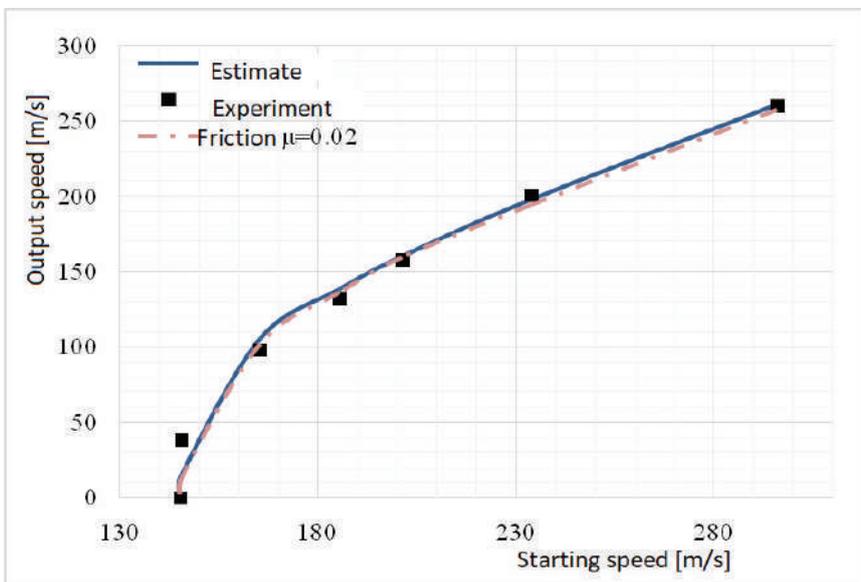
Figure 12 – FEM analysis by a blunt projectile for a plate of 6 mm thickness
Рис. 12 – Анализ FEM тупоконечным снарядом на плиту, толщиной 6 мм
*Слика 12 – Анализа ФЕМ тупим пројектилом за плочу дебљине 6 тт*
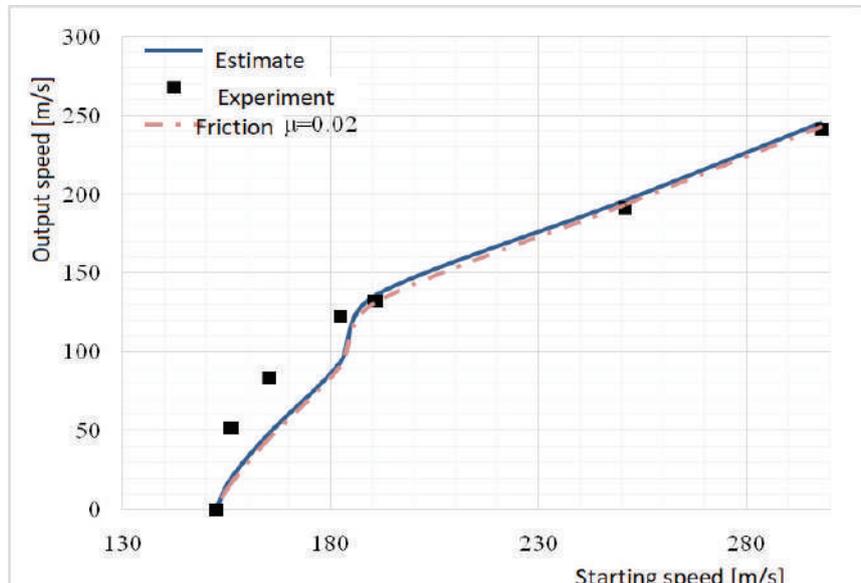
Figure 13 – FEM analysis by a blunt projectile for a plate of 8 mm thickness
Рис. 13 – Анализ FEM тупоконечным снарядом на плиту, толщиной 8 мм
Слика 13 – Анализа ФЕМ тупим пројектилом за плочу дебљине 8 тт
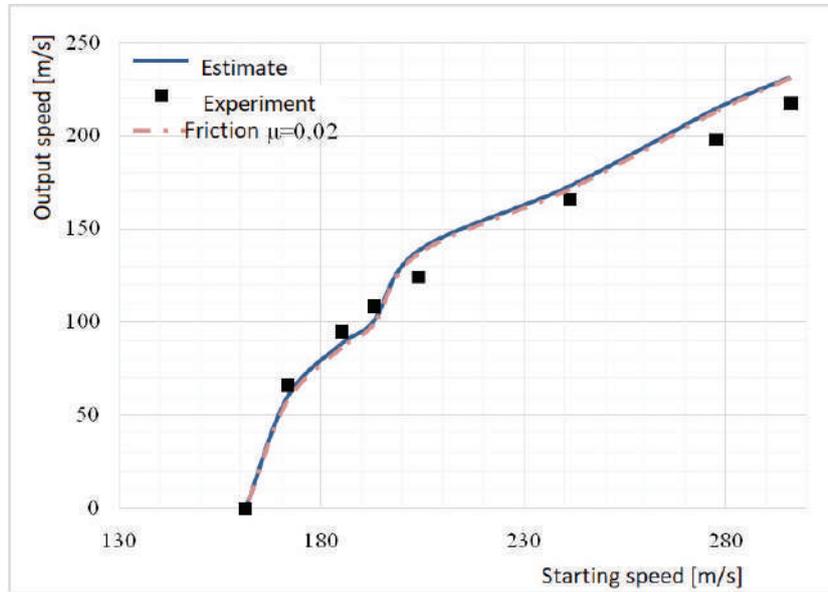
Figure 14 – FEM analysis by a blunt projectile for a plate of 10 mm thickness
Рис. 14 – Анализ FEM тупоконечным снарядом на плиту, толщиной 10 мм
Слика 14 – Анализа ФЕМ тупим пројектилом за плочу дебљине 10 mm
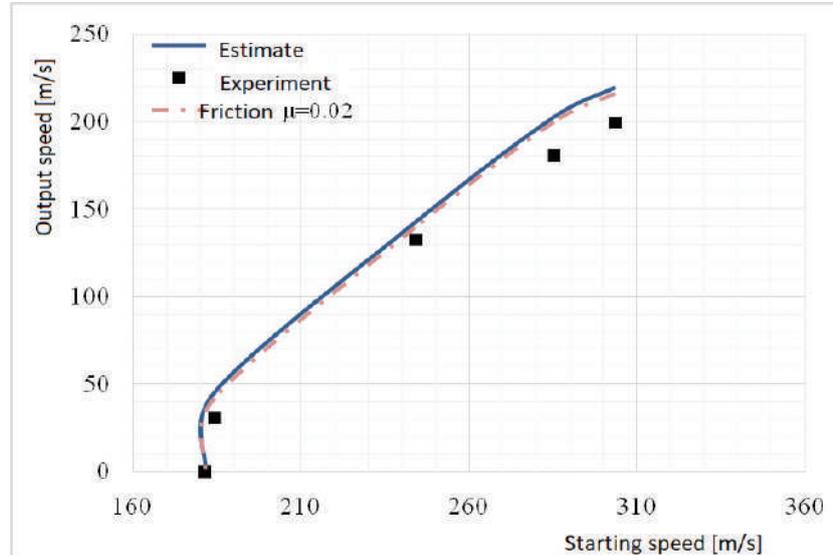
Figure 15 – FEM analysis by a blunt projectile for a plate of 12 mm thickness
Рис. 15 – Анализ FEM тупоконечным снарядом на плиту, толщиной 12 мм
Слика 15 – Анализа ФЕМ тупим пројектилом за плочу дебљине 12 mm
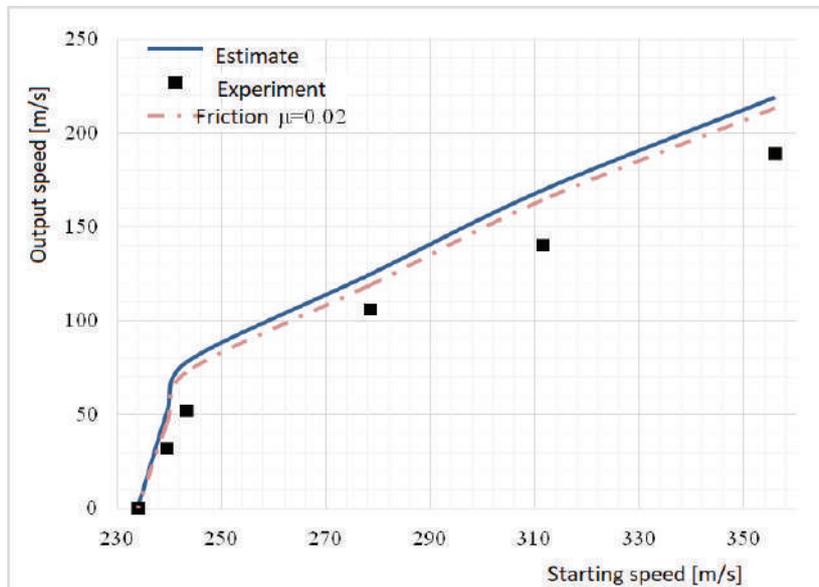
Figure 16 – FEM analysis by a blunt projectile for a plate of 16 mm thickness
Рис. 16 – Анализ FEM тупоконечным снарядом на плиту, толщиной 16 мм
Слика 16 – Анализа ФЕМ тупим пројектилом за плочу дебљине 16 mm
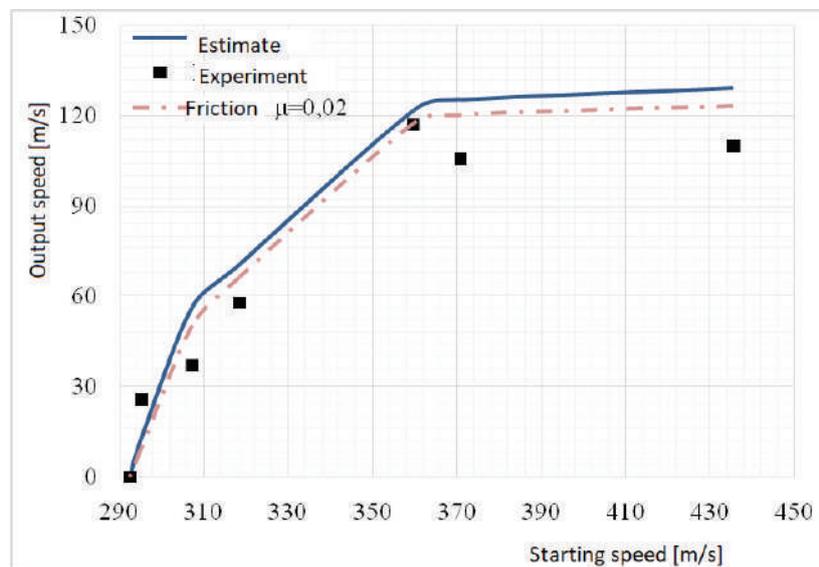
Figure 17 – FEM analysis by a blunt projectile for a plate of 20 mm thickness
Рис. 17 – Анализ FEM тупоконечным снарядом на плиту, толщиной 20 мм
Слика 17 – Анализа ФЕМ тупим пројектилом за плочу дебљине 20 mm

An analysis of the FEM method for ballistic boundary velocities was performed. These velocities are defined as the minimum speeds of the projectiles needed to penetrate a fully targeted board. It has been confirmed that the FEM method provides good agreement with experimental results in all of the examined thicknesses. The numerical analysis of the blunt projectile, as shown in the 2D model in Figure 18 and the 3D model in Figure 19, shows that the correct simulation was performed and a proper cut after the break of the plate as well as experimental effects was obtained.

Figure 20 shows the results of the temperature change and the effect of the temperature on the plate perforation. It can be clearly seen from the figure that the temperature is highest in the part of the edges of the projectiles and boards. It can be seen from the figure that the breakage of the plate is caused by the ductile expansion of the hole and the breakthrough due to the flow of the material of the plate as a result of the adiabatic shear of the temperature. A similar behavior is observed in other cases for which the calculations were carried out. The effect of damage by changing the speed obtained by a numerical analysis is shown in Figure 21, for an initial velocity of $V_0 = 296$ [m/s], indicates the change in the damage of the steel plate from the initial part where the speed is slowly slowing down and linearly decreasing until the moment of plate breakage.
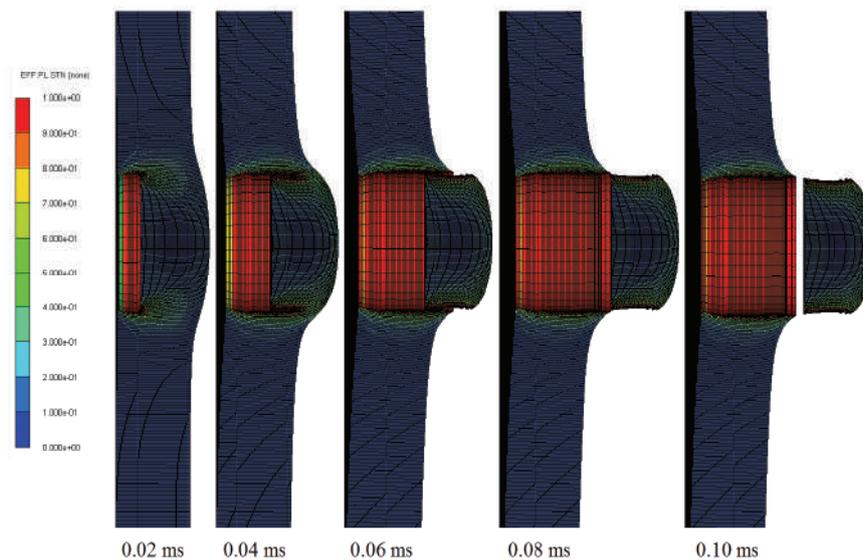
Figure 18 – Perforation of a steel plate with a blunt projectile (FEM method)
Рис. 18 – Перфорация стальной плиты тупоконечным снарядом (FEM метод)
*Слика 18 – Перфорација челичне плоче тупим пројектилом (ФЕМ метода)*
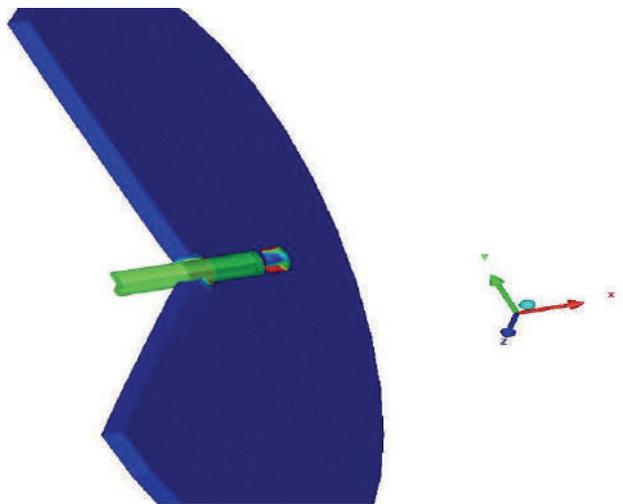
Figure 19 – 3D Flat Perforation of a steel shell with a blunt projectile (FEM Method)
Рис. 19 – Изображение 3Д перфорации стальной плиты тупоконечным снарядом (FEM метод)
Слика 19 – Приказ 3D перфорације челичне плоче тупим пројектилом (ФЕМ метода)
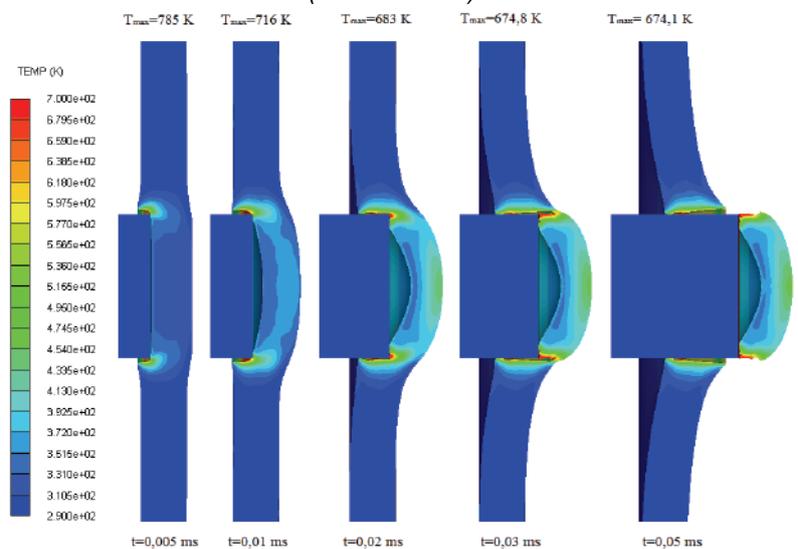

Figure 20 – Analysis of the change in the temperature field during the breakdown of the steel plate by a blunt projectile (FEM method)
Рис. 20 – Анализ изменений теплового поля при пробое стальной плиты тупоконечным снарядом (FEM метод)
Слика 20 – Анализа промене температурног поља при пробоју челичне плоче тупим пројектилом (ФЕМ метода)
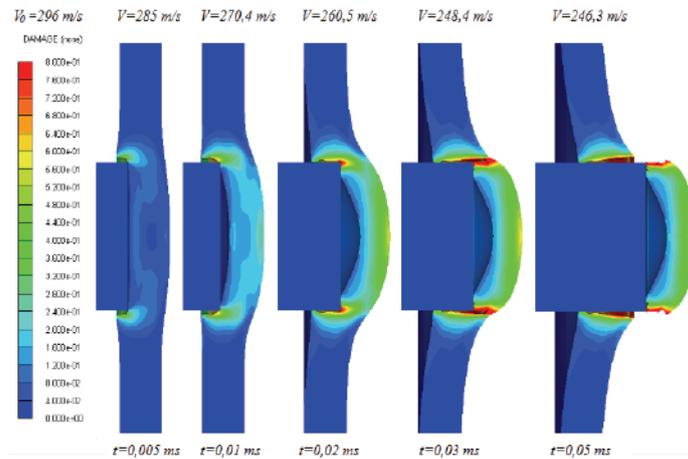
Figure 21 – Analysis of damage caused by the change of speed in the breakdown of the steel plate by a blunt projectile (FEM method)
Рис. 21 – Анализ повреждений и изменения скорости при пробое стальной плиты тупоконечным снарядом (FEM метод)
Слика 21 – Анализа оштећења са променом брзине при пробоју челичне плоче тупим пројектилом (ФЕМ метода)

Comparative analysis of the FEM and SFM methods

By comparing the FEM and SFM methods based on the convergence study for the adopted elements of 0.25x0.25x0.25 mm^3 for modeling the target board in the SFM mode, the impact of the projectile and the network is gradually shifted to the outer edge. The obtained FEM results, together with the SFM values, predict a change in inclination similar to those observed in previous experiments. Figures 22, 23 and 24 show a comparative analysis of the numerical simulation results of the FEM and SFM methods with the same initial speeds, by the action of a blunt projectile for the plate thicknesses of 6 mm, 8 mm and 16 mm.
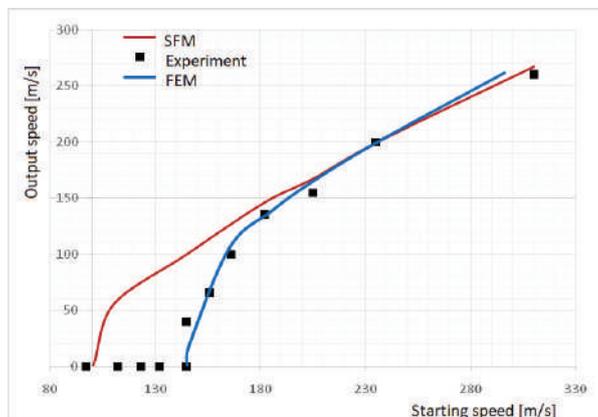
Figure 22 – Comparison of the results obtained by the FEM and SFM methods
for a 6 mm thick steel plate, with a blunt projectile
Рис. 22 – Сравнительный анализ результатов, полученных FEM и SFM
методами, выполненных на основании повреждений стальной плиты толщиной
6 мм, пораженной тупоконечным снарядом
Слика 22 – Поређење резултата добијених ФЕМ и СФМ методом за челичну
плочу дебљине 6 mm пробијену тупим пројектилом
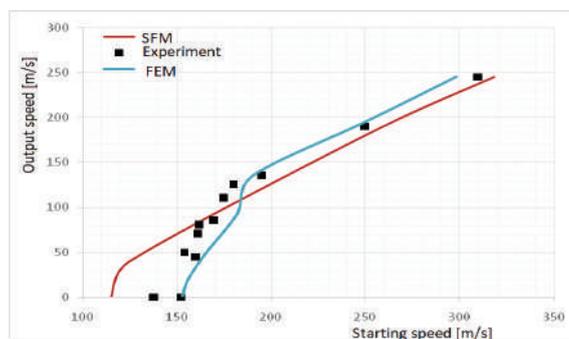
Figure 23 – Comparison of the results obtained by the FEM and SFM methods for
an 8 mm thick steel plate with a blunt projectile
Рис. 23 – Сравнительный анализ результатов, полученных FEM и SFM
методами, выполненных на основании повреждений стальной плиты толщиной
8 мм, пораженной тупоконечным снарядом
Слика 23 – Поређење резултата добијених ФЕМ и СФМ методом за челичну
плочу дебљине 8 mm пробијену тупим пројектилом
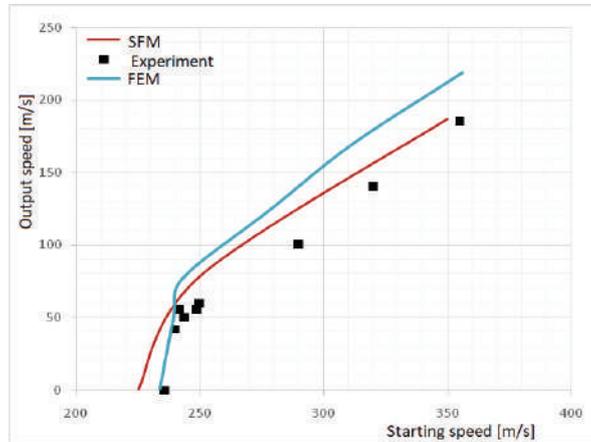
*Figure 24 – Comparison of the results obtained by the FEM and SFM methods
for a 16 mm thick steel plate with a blunt projectile
Рис. 24 – Сравнительный анализ результатов, полученных FEM и SFM
методами, выполненных на основании повреждений стальной плиты толщиной
16 мм, пораженной тупоконечным снарядом
Слика 24 – Поређење резултата добијених ФЕМ и СФМ методом за челичну
плочу дебљине 16 mm пробијену тупим пројектилом*

From the diagram, it can be noticed that the results obtained by the FEM and SFM methods for the plates of small thicknesses overlap in the initial part; however, in the final part, near the boundary ballistic velocities, the SFM method has minor deviations. In the numerical analysis for the SFM method (Fig. 34) an irregular shape of the separation of the rear part of the plate is seen, and in some cases, the breakdown and breakage of the plate. For the thicknesses above 10 mm, the matching of the results is within the limits of tolerance in all phases of the projectile penetration, which was also shown for the penetration of the blunt projectile by the SFM method for a plate of 16 mm in thickness.

Perforation of aluminum plates

This part of the paper deals with a perforation of AA5083-H116 aluminum plates with a thickness of 15 mm to 30 mm with a conical tip projectile. The software used for the analyses presented in this paper is 2D and 3D Autodyn for two-dimensional and three-dimensional problems, respectively, in their original form. Numerical natural velocities of projectiles and ballistic boundary velocities are compared with the experimental data previously published by (Borvik et al, 2003, pp.413-464), (Borvik et al, 2004, pp.367-384). The variation of the natural velocities at the initial speeds for different plate thicknesses of 15, 20, 25 and 30 mm is represented from Figures 25 to 28. The ballistic boundary velocities increase

linearly by increasing the thickness of the plates, as shown in the above figures, showing a similar fracture pattern to the plates of all thicknesses.
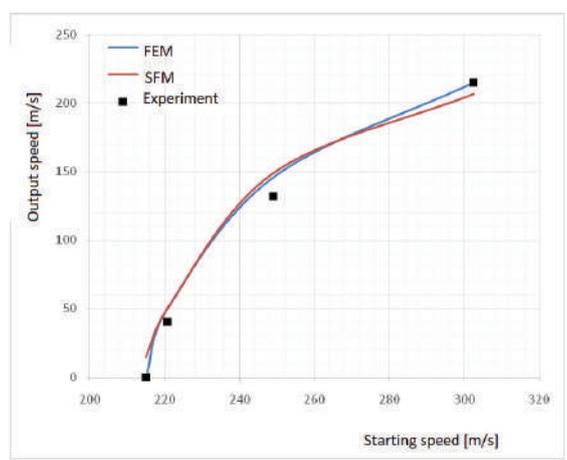

Figure 25 – Comparison of the results obtained with the FEM and SFM methods for an aluminum plate with a thickness of 15 mm, conical projectile
Рис. 25 – Сравнительный анализ результатов, полученных FEM и SFM методами, выполненных на основании повреждений алюминиевой плиты толщиной 15 мм, пораженной остроконечным снарядом
Слика 25 – Поређење резултата добијених ФЕМ и СФМ методом за алуминијумску плочу дебљине 15 mm пробијену конусним пројектилом
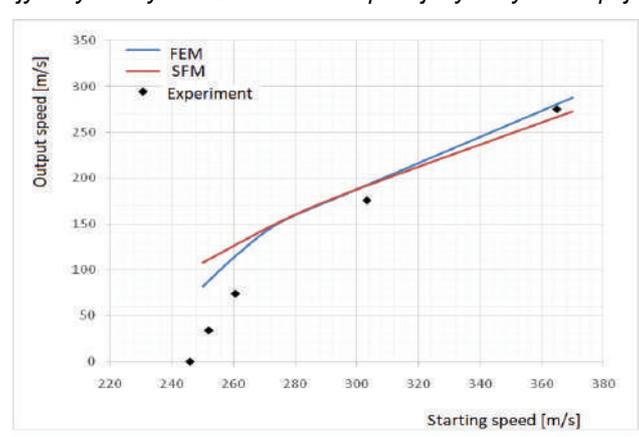

Figure 26 – Comparison of the results obtained with the FEM and SFM methods for an aluminum plate with a thickness of 20 mm, conical projectile
Рис. 26 – Сравнительный анализ результатов, полученных FEM и SFM методами, выполненных на основании повреждений алюминиевой плиты толщиной 20 мм, пораженной остроконечным снарядом
Слика 26 – Поређење резултата добијених ФЕМ и СФМ методом за алуминијумску плочу дебљине 20 mm пробијену конусним пројектилом
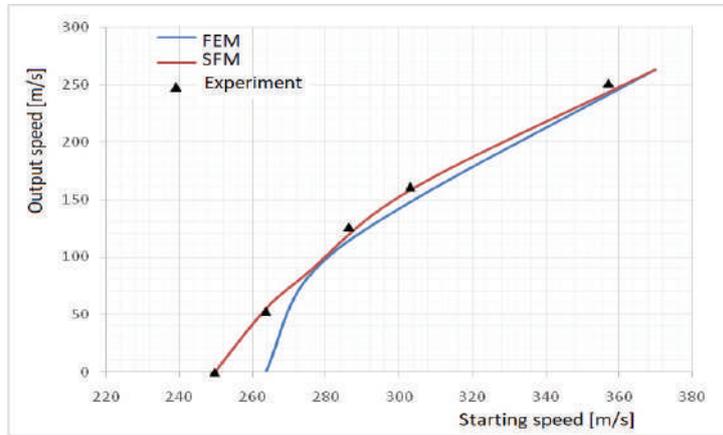
Figure 27 – Comparison of the results obtained with the FEM and SFM methods for an aluminum plate with a thickness of 25 mm, conical projectile
Рис. 27 – Сравнительный анализ результатов, полученных FEM и SFM методами, выполненных на основании повреждений алюминиевой плиты толщиной 25 мм, пораженной остроконечным снарядом
Слика 27 – Поређење резултата добијених ФЕМ и СФМ методом за алуминијумску плочу дебљине 25 mm пробијену конусним пројектилом
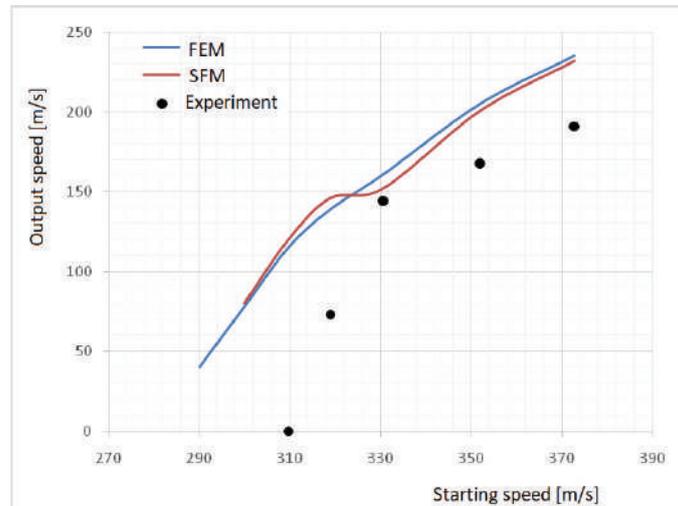
Figure 28 – Comparison of the results obtained with the FEM and SFM methods for an aluminum plate with a thickness of 30 mm, conical projectile
Рис. 28 – Сравнительный анализ результатов, полученных FEM и SFM методами, выполненных на основании повреждений алюминиевой плиты толщиной 30 мм, пораженной остроконечным снарядом
Слика 28 – Поређење резултата добијених ФЕМ и СФМ методом за алуминијумску плочу дебљине 30 mm пробијену конусним пројектилом

The analyses were made for a range of initial velocities from 200 m/s to 400 m/s. The thickness of aluminum plates varies from 15 mm, 20 mm, 25 mm and 30 mm. The output velocity of the projectile was measured when the projectile speed at the perforation after the output from the plate stabilized. The obtained results were compared with the experimental results obtained by (Borvik et al, 2003, pp.413-464), (Borvik et al, 2004, pp.367-384). In the previous diagrams (Figures 25-28), a comparison of the results for the FEM and SFM with the experimental results is shown. It is noticeable that the SFM results are closer to the experimental data, which is characteristic for softer plates. Figure 29 shows effective plastic deformation for the SFM method at different time intervals when perforating a 20 mm thick aluminum plate with an initial initial velocity V_0 = 370 [m/s]. The Figures show that the plate is penetrated due to the ductile expansion of the hole. A similar behavior is also observed in the FEM method (Figure 30) for a 15mm thick plate with the initial initial projectile velocity V_0 = 302 [m/s], with an expressed part of the adiabatic shear, which is the case with other thicknesses for which the calculations were performed.
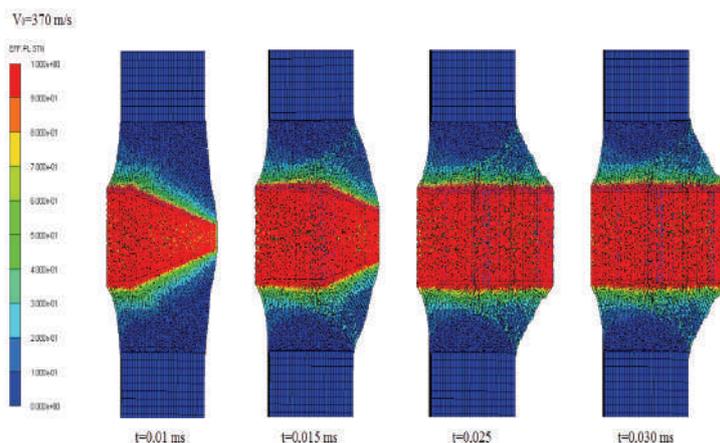

Figure 29 – Perforation of a 20 mm thick aluminum plate by a conical projectile (SFM method)
Рис. 29 – Изображение пробоя алюминиевой плиты, толщиной 20 мм, пораженной остроконечным снарядом (SFM метод)
Слика 29 – Приказ перфорације алуминијумске плоче дебљине 20 mm настале услед пробијања конусним пројектилом (СФМ методом)
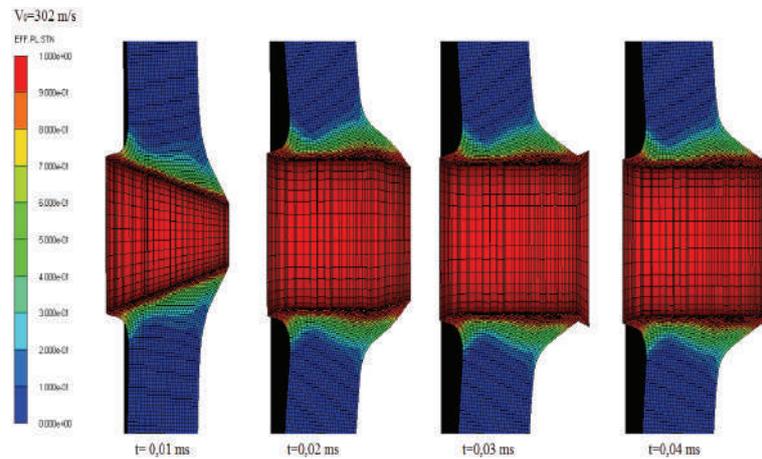
Figure 30 – Perforation of a 15 mm thick aluminum plate by a conical projectile (SFM method)
Рис. 30 – Изображение пробоя алюминиевой плиты, толщиной 15 мм, пораженной остроконечным снарядом (SFM метод)
Слика 30 – Приказ перфорације алуминијумске плоче дебљине 15 mm настале услед пробијања конусним пројектилом (СФМ методом)

Perforation of projectiles of various tip geometries

This part of the paper analyses the perforation of a 12 mm thick Weldox 460E steel plate by a blunt, conical and hemispherical tip of the projectile. Numerical average and ballistic boundary velocities are compared with the experimental data from literature. It has been confirmed that the numerical results are in good agreement with the experimental data, as shown in Table 4. The results obtained for ballistic bound velocities using the FEM method show that, for the tested cases, less than 6% of the experimental data deviate.

Table 4 – Ballistic boundary velocity (Vbl) for three different projectiles
Таблица 4 – Баллистическая граничная скорость (Vbl) трех различных видов снарядов
Табела 4 – Балистичка гранична брзина (V_{bl}) за три различита пројектила

Ballistic boundary velocity, Vbl (m/s)	blunt	cone	hemispheric
Experiment	181.5	280.9	292.1
FEM	181.5	265.0	292.1

The numerical simulation of the penetration of a 12 mm thick steel plate with three projectiles of different tip geometry, as shown in the diagram (Figure 31), showed good agreement with the experimental results shown by Dey in his scientific work.

The numerical analysis has shown that conical and hemispherical projectiles have a characteristic of faster penetration through various types of obstacles (plates) by shifting the material in radial direction and by increasing the plastic hole, as shown in Figures 32 and 33. For the same hemispherical projectile, the SFM method shows the surface of a steel plate at a time from t = 0.0 ms to t = 0.12 ms. At a time of t = 0.06 ms, the surface of the steel plate rear begins to irregularly disintegrate, and at the very end of the plate, separation (splitting) is increasingly observed at the exit from the plate. The calculations were stopped at a time interval t = 0.12 ms, when the projectile penetrated the plate.

For blunt projectiles, plate penetration occurs with adiabatic cleavage and compression where the thickness of the compressed section is similar to that of the plate and leaf flattening detected on the rear surface shown in Figure 34, which is characteristic for the application of the SFM method in a numerical analysis of a blunt projectile effect on a hard steel plate.
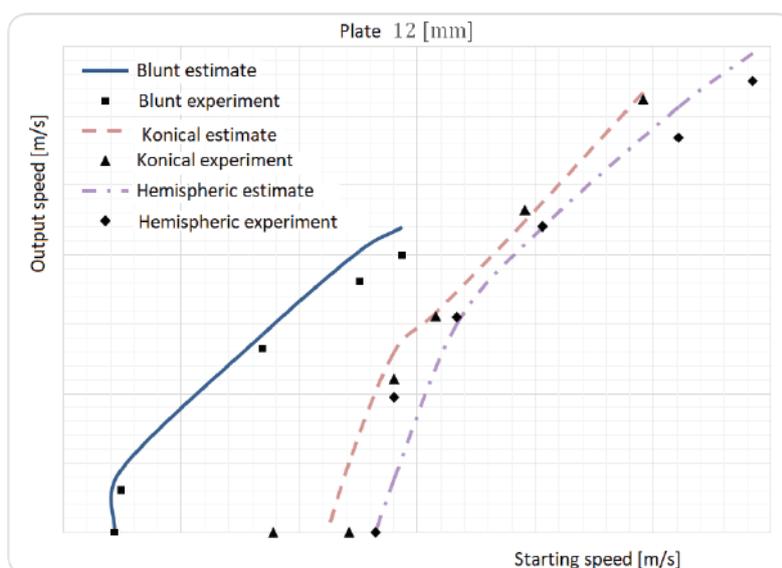

Figure 31 – Comparison of experimental, average values of numerical and ballistic boundary velocities
Рис. 31 – Сравнение экспериментальной, средней численной и баллистической граничной скорости
*Слика 31 – Поређење експерименталних, просечних вредности нумеричких и балистичких граничних брзина*
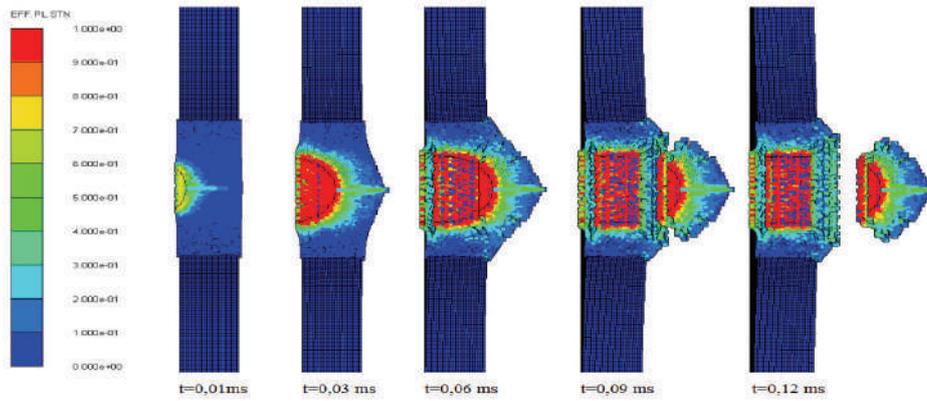
Figure 32 – Perforation of a 12 mm thick steel plate, hemispherical projectile (SFM method)
Рис. 32 – Пробой стальной плиты, толщиной 12 мм, хемисферическим снарядом (SFM метод)
Слика 32 – Перфорација челичне плоче дебљине 12 mm, настала услед пробијања хемисферичним пројектилом (СФМ метода)
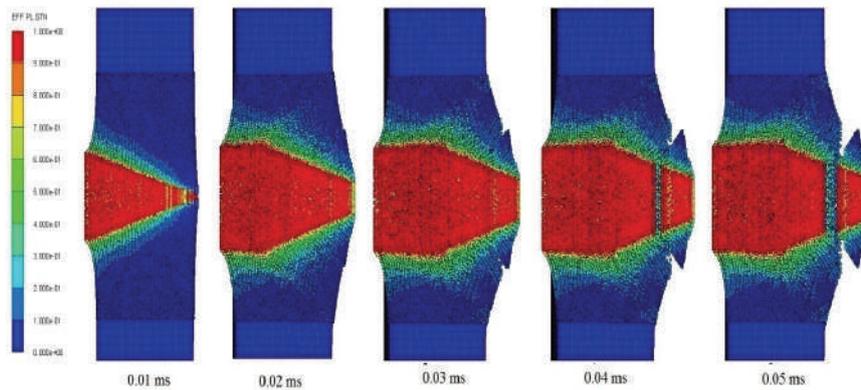

Figure 33 – Perforation of a 15 mm thick steel plate, hemispherical projectile (SFM method)
Рис. 33 – Пробой стальной плиты, толщиной 15 мм, хемисферическим снарядом (SFM метод)
Слика 33 – Перфорација челичне плоче дебљине 15 mm, настала услед пробијања хемисферичним пројектилом (СФМ метода)
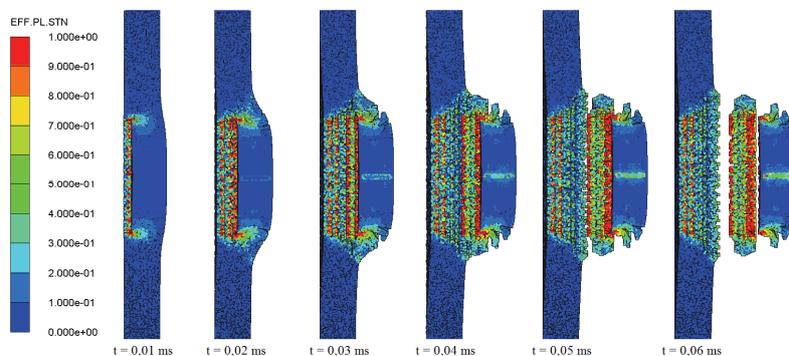
Figure 34 – Perforation of a 6 mm thick steel plate, hemispherical projectile (SFM method)

Рис. 34 – Пробой стальной плиты, толщиной 6 мм, хемисферическим снарядом (SFM метод)

Слика 34 – Перфорација челичне плоче дебљине 6 mm, настала услед пробијања хемисферичним пројектилом (СФМ метода)

The results obtained by numerical simulations included the effect of damaging the steel plate of various thicknesses by the action of projectiles of different shapes of the tips (noses), as shown in Figs. 35 to 38. The indicated damage regimen for each verified case is within the limits of the experimental results given in the literature used. The analysis was performed with a blunt projectile for two different plate thicknesses (6 and 16 mm), by simulating average speeds (296 and 356 m/s) and limit speeds (145 and 239 m/s), as shown in Figures 35 and 36. From the analysis of the results, it can be seen that by the action of a blunt projectile, the initiation of the adiabatic shear range appears very quickly, due to the geometric singularity of the projectile, after several milliseconds. Such a range of adiabatic shear creates a plug that is ejected during the final break of the plate. It can be seen form the Figure that the higher speed is, the sooner the plate breaks down, and the section created by the adiabatic shear is thinner at higher speeds. Also, it was noticed that with the impact of the projectiles of the same caliber on 6 mm thin plates (Figure 35), and for lower speeds (near the ballistic velocity), plate bending was three times more expressed. In order to compare the results for the 16 mm thick plate (Figure 36), an analysis was performed for two different speeds and it was confirmed, as in thinner plates, that at higher speeds penetration occurs faster and there is a difference in the thickness of the cutoff after penetration, which is visible in the Figure. However, it was noticed in thicker plates that the "plate-like" twisting was significantly less prominent than in thinner plates (see Figure 36).

From the analysis of the results, it can be seen that a conical projectile penetrates the plate significantly earlier. Also, in these types of projectiles,

adiabatic shear is generated, but a plug is not formed when the plate is penetrated (Figure 37). It can be seen from the Figure that the higher the speed is, the sooner penetration occurs, as in the case of a blunt projectile. When the same caliber projectile penetrates a thin plate of 6 mm (Fig. 37) at lower speeds (near the boundary ballistic velocity), plate bending is two times more prominent. For the hemispherical projectile nose (Figure 38), the results also showed that for a plate of 6 mm thickness, simulation of the action at two different speeds confirmed that the thinner plates were faster to break and there was a difference in the thickness of the cutoff after plate penetration (as seen in the Figure). However, it was noticed that, at lower speeds, there would be a "plate-like" twist as in the case of a blunt projectile, as shown in Figure 38.
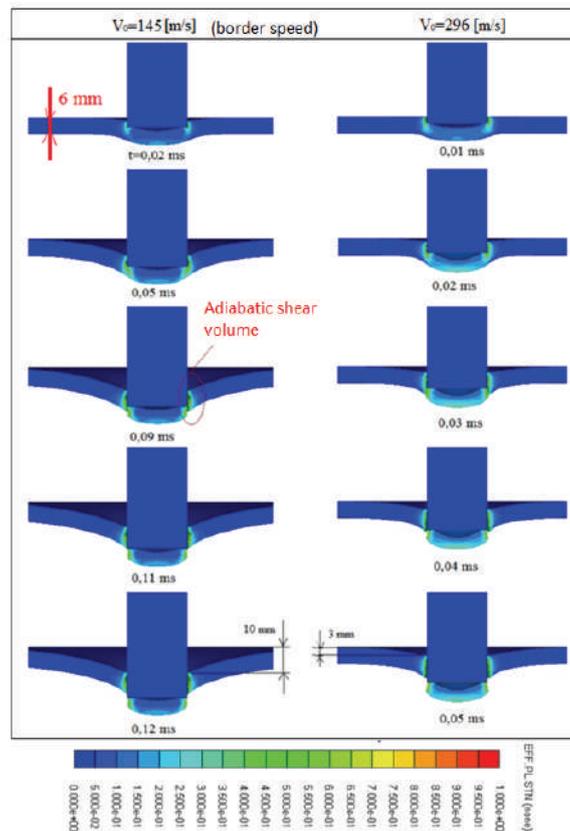

Figure 35 – Comparison of blunt projectile penetration through a 6mm-thick steel plate at two speeds, Vo=145 m/s and Vo=296 m/s, FEM method
Рис. 35 – Сравнительное изображение пробоя стальной плиты, толщиной 6мм тупоконечным снарядом с двумя скоростями: Vo=145 m/s и Vo=296 m/s, FEM метод
Слика 35 – Упоредни приказ пробоја челичне плоче дебљине 6 mm тупим пројектилом при брзинама Vo=145 m/s и Vo=296 m/s, ФЕМ методом
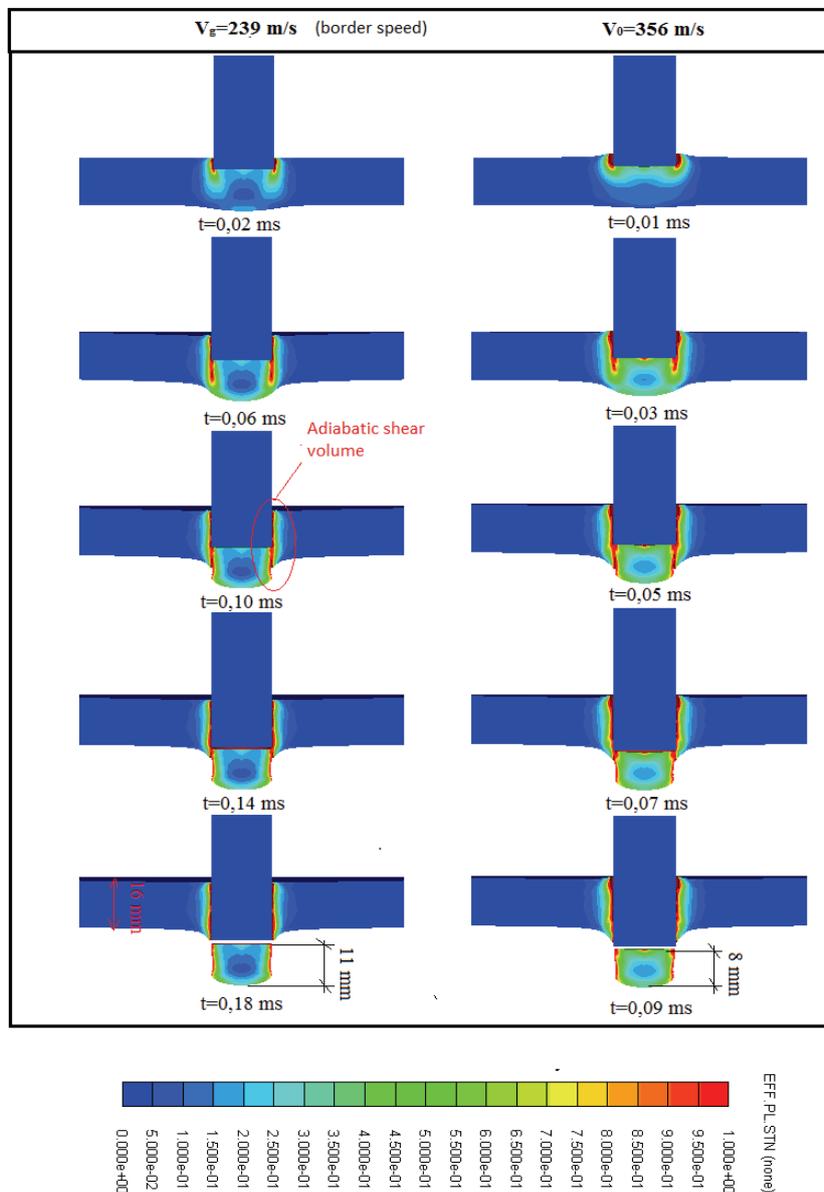
Figure 36 – Comparison of blunt projectile penetration through a 16mm-thick steel plate
at two speeds, Vo=239 m/s and Vo=356 m/s, FEM method
Рис. 36 – Сравнительное изображение пробоя стальной плиты, толщиной 16мм
тупоконечным снарядом с двумя скоростями: Vo=239 m/s и Vo=356 m/s, FEM метод
Слика 36 – Упоредни приказ пробоја челичне плоче дебљине 16 mm тупим
*пројектилом при брзинама Vo=239 m/s и Vo=356 m/s , ФЕМ методом*
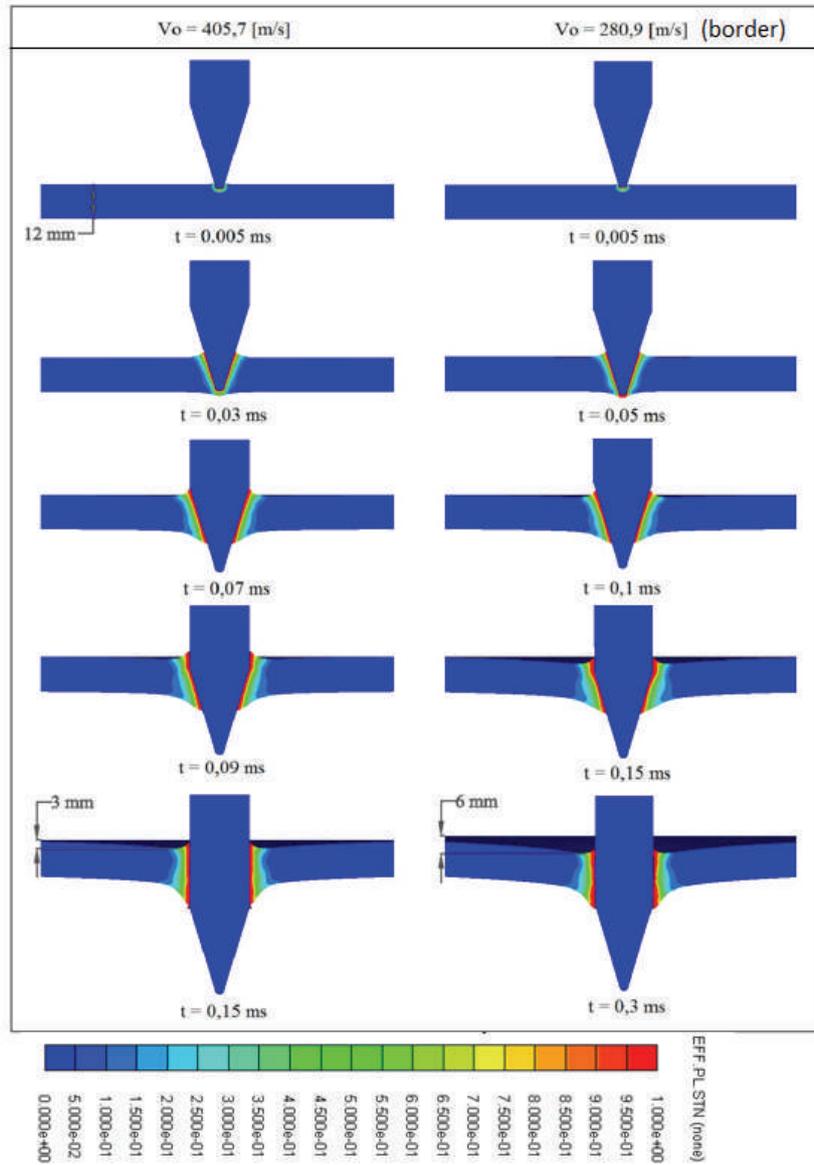
Figure 37 – Comparative illustration of steel plate penetration by two-speed cone projectiles, FEM method
Рис. 37 – Сравнительное изображение пробоя стальной плиты остроконечным снарядом с двумя скоростями, FEM метод
Слика 37 – Упоредни приказ пробоја челичне плоче конусним пројектилом са две брзине, ФЕМ методом
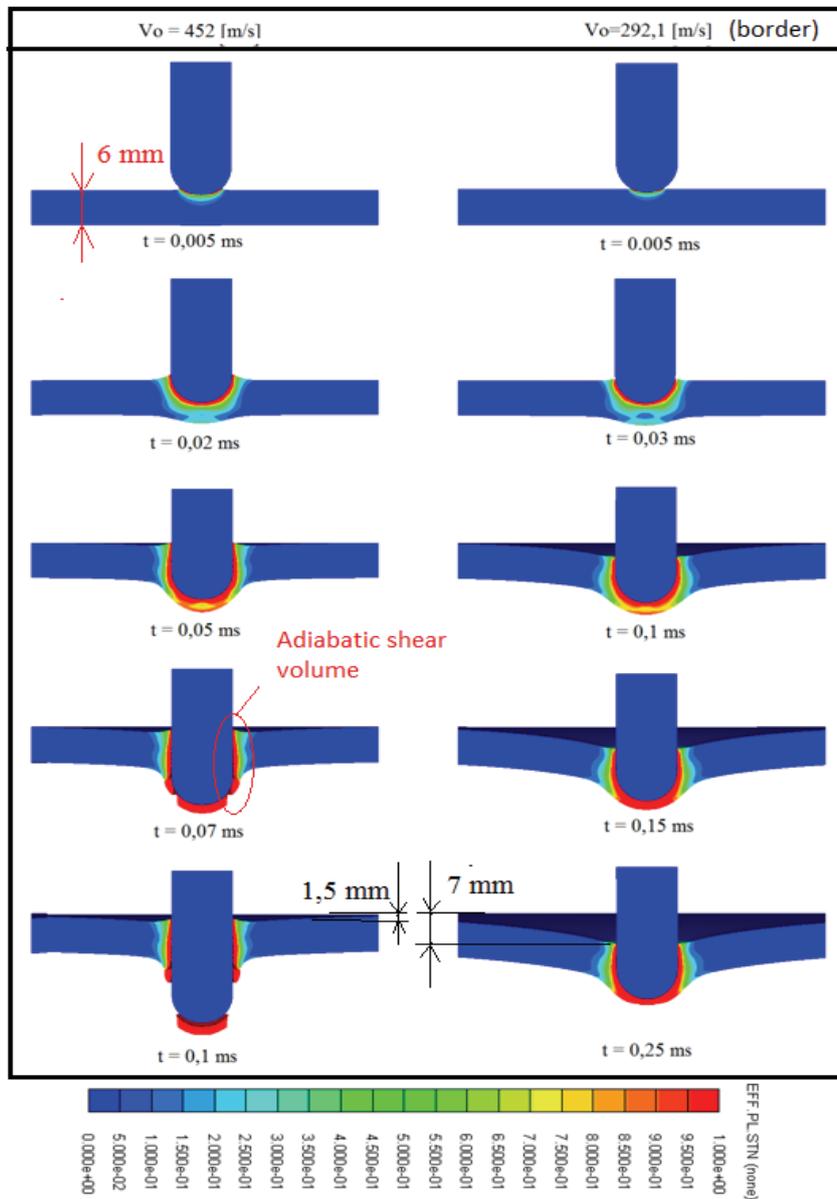
Figure 38 – Comparative illustration of steel plate penetration by two-speed hemispherical projectiles, FEM method

Рис. 38 – Сравнительное изображение пробоя стальной плиты хемисферическим снарядом с двумя скоростями, FEM метод

Слика 38 – Упоредни приказ пробоја челичне плоче хемисферичним пројектилом са две брзине, ФЕМ методом

The presented results were obtained by the coupled SPH-FEM method (SFM) and the FEM, which were adopted for simulating the perforation of steel and aluminum plates of various thicknesses at high speeds, with steel projectiles of different noses. It has been confirmed that both methods can predict fairly accurate fracture patterns, natural missile speeds, and ballistic boundary velocities compared to those observed in previously published analyses of impacts of different types of projectile tips. The deviation in the results was observed for the perforation of thin plates with a blunt projectile using the SFM method. However, changes in the fracture pattern do not fully reflect in the solution obtained from the adopted method, except for smaller impact speeds on thin plates, and these changes occur due to the problem of unstable load which is characteristic for the SFM method. With a reduced range of impact velocities, FEM solutions are in better agreement with experiments and can be adopted for this range of impact velocities. The SFM method combines the benefits of the SPH and FEM methods, while solving their shortcomings in the demanding (at higher speeds) processing and early end of the program due to the serious interruption of the original elements from the real application. Although the SFM is less accurate at lower impact speeds of 170 m/s and less, the method is suitable and efficient for numerically analysing high-velocity penetration and perforation of softer materials, such as aluminum plates.

The Johnson-Cook constituent model and the finite element method, as well as the coupled method (FEM and SFM), were used to perform a numerical analysis of the impacts of a steel projectile on aluminum plates at high velocities. The analyses have shown that there is fairly good agreement with the experimental data for smaller thickness plates, while smaller deviations occur in plates with larger thickness. Also, numerical results deviate more from the experimental ones in the area of lower impact velocities. In order to improve the numerical model and bring the obtained results closer to the experimental ones, it is possible to introduce the influence of the temperature change in the Johnson-Cook constitutive material strength model on plates of larger thicknesses and introduce the influence of friction that occurs during the interaction between projectiles and plates.

Conclusion

The research includes modern methods for modeling impact damage based on the combined application of methods developed by theoretical, experimental and numerical tools. Various types of impacts are analysed numerically. Defined numerical models were applied for the analysis of normal

impacts of projectiles with different types of steel and aluminum tips for a wide impact speed range. Different thicknesses of obstacles were used for the analyses (Weldox steel plate from 6 to 20 mm, aluminum plates from 10 to 25 mm). By varying geometric shapes and materials, wide possibilities have been created for the numerical analysis of various phenomena occurring during the impact, previously identified by experimental tests. By combining the numerical analysis, the theoretical results and the experimental tests, it is possible to gain a wider insight into the processes that occur in impact damage on different metal structures.

An insight gained through the research of analytical and empirical models of impacts on metal structures has helped develop numerical models for more complicated geometry conditions and different structures and surfaces.

During the research, numerical methods based on the finite element method (FEM) and the method based on the coupling of the smooth particle hydrodynamics method and the finite element method (SFM) were applied. It has been confirmed that both methods can predict the exact shape of a fracture, the natural velocity of the projectile, and the ballistic boundary velocity in comparison with those observed in the previously published analyses on the impacts of different projectile nose shapes, with the limits of the application of both methods. The deviation in the results was observed for the perforation of hard steel plates by blunt projectiles using the SFM method. However, disagreements in the predicted fracture shape have no greater impact on the calculated output speeds, except for lower impact speeds on thin plates. At impact speeds that are close to the ballistic ballistic velocity of the FEM solution, they are in better agreement with experiments and can be adopted for the interval of impact velocities applied in the analysis. The SFM method combines the advantages of the SPH and FEM method, overcoming the problem related to the inability to realise the FEM calculation due to the excessive deformation of the numerical network, which is particularly expressed in complex geometric shapes. Although the SFM is less accurate at lower impact speeds, the method is suitable and efficient enough for the numerical analysis of high-velocity penetration and perforation of softer materials such as aluminum plates, whereby with minimal increase in the required computation time, problems with excessive deformation of numerical networks are avoided. Using the Johnson-Cook constituent model for fracture models and materials, the results are obtained that are in good agreement with the corresponding experiments for both applied numerical methods. The analyses for the aluminum plate have shown that for smaller thicknesses there are fairly good matches with the experimental data, while there are significant deviations in plates of larger thicknesses. Also, the numerical results deviate more from the experimental ones in the area of lower impact velocities. In order to improve the numerical model and the obtained results closer to the experimental

ones, in the case of larger thicknesses it is possible to introduce the influence of temperature change in the JS constitutive material strength model and to introduce the influence of friction that occurs during the interaction of the projectile and the plate.

The results are shown for the perforation by missiles with different noses, showing the influence of temperature, plastic deformations, speed of plastic deformations, shear and velocity for projectile penetration through steel and aluminum plates of different thicknesses (from 6-25 mm).

References

Anderson, C.E., 1987. An overview of the theory of hydrocodes. *International Journal of Impact Engineering*, 5(1-4), pp.33-59. Available at: https://doi.org/10.1016/0734-743X(87)90029-7.

Anderson, C.E., Cox, P.A., Johnson, G.R. & Maudlin, P.J., 1994. A constitutive formulation for anisotropic materials suitable for wave propagation computer programs—II. *Computational Mechanics*, 15(3), pp.201-223. Available at: https://doi.org/10.1007/BF00375030.

Anderson, T.A., 2005. An investigation of SDOF models for large mass impact on sandwich composites. *Composites Part B: Engineering*, 36(2), pp.135-142. Available at: https://doi.org/10.1016/j.compositesb.2004.05.002.

Backman, M.E. & Goldsmith, W., 1978. The mechanics of penetration of projectiles into targets. *International Journal of Engineering Science*, 16(1), pp.1-99. Available at: https://doi.org/10.1016/0020-7225(78)90002-2.

Borvik, T., Hopperstad, O.S., Langseth, M. & Malo, K.A., 2003. Effect of target thickness in blunt projectile penetration of Weldox 460 E steel plates. *International Journal of Impact Engineering*, 28(4), pp.413-464. Available at: https://doi.org/10.1016/S0734-743X(02)00072-6.

Borvik, T., Clausen, A.H., Hopperstad, O.S. & Langseth, M., 2004. Perforation of AA5083-H116 aluminium plates with conical-nose steel projectiles: Experimental study. *International Journal of Impact Engineering*, 30(4), pp.367-384. Available at: https://doi.org/10.1016/S0734-743X(03)00072-1.

Clausen, A.H., Borvik, T., Hopperstad, O.S. & Benallal, A., 2004. Flow and fracture characteristics of aluminium alloy AA5083-H116 as function of strain rate, temperature and triaxiality. *Materials Science and Engineering*, 364(1-2), pp.260-272. Available at: https://doi.org/10.1016/j.msea.2003.08.027.

Dey, S., 2004. *High-strength steel plates subjected to projectile impact: An experimental and numerical study*, Ph.D. thesis, Norwegian University of Science and Technology, ISBN 82-471-6282-2.

Gingold, R.A. & Monaghan, J.J., 1977. Smoothed particle hydrodynamics: Theory and application to nonspherical stars. *Monthly Notices of the Royal*

Astronomical Society, 181(3), pp.375-389. Available at: https://doi.org/10.1093/mnras/181.3.375.

Johnson, G.R. & Cook, W.H., 1985. Fracture characteristics of three metals subjected to various strains, strain rates, temperatures and pressures. *Engineering Fracture Mechanics,* 21(1), pp.31-48. Available at: https://doi.org/10.1016/0013-7944(85)90052-9.

Lee, M. & Yoo, Y.H., 2001. Analysis of ceramic/metal armour system. *International Journal of Impact Engineering,* 25(9), pp.819-829. Available at: https://doi.org/10.1016/S0734-743X(01)00025-2.

Lucy, L.B., 1977. A numerical approach to the testing of the fission hypothesis. *Astronomical Journal,* 82, pp.1013-1024. Available at: https://doi.org/10.1086/112164.

Ravid, M. & Bodner, S.R., 1983. Dynamic perforation of viscoplastic plates by rigid projectiles. *International Journal of Engineering Science,* 21(6), pp.577-591. Available at: https://doi.org/10.1016/0020-7225(83)90105-2.

Rosenberg, Z. & Tsaliah, J., 1990. Applying Tate's model for the interaction of long rod projectiles with ceramic targets. *International Journal of Impact Engineering,* 9(2), pp.247-251. Available at: https://doi.org/10.1016/0734-743X(90)90016-O.

Rosenberg, Z. & Yeshurun, Y., 1988. The relation between ballistic efficiency andcompressive strength of ceramic tiles. *International Journal of Impact Engineering,* 7(3), pp.357-362. Available at: https://doi.org/10.1016/0734-743X(88)90035-8.

Spasić, D., 2015. *Modelovanje udarnih oštećenja vazduhoplovnih struktura,* Ph.D. thesis, University in Belgrade: Faculty of Mechanical Engineering (in Serbian).

Taylor, G.I., 1948. The formation and enlargement of a circular hole in a thin plastic sheet. *Quarterly Journal of Mechanics and Applied Mathematics,* 1(1), pp.103–124. Available at: https://doi.org/10.1093/qjmam/1.1.103.

ЧИСЛЕННОЕ МОДЕЛИРОВАНИЕ УДАРА СНАРЯДА
ПО МЕТАЛЛИЧЕСКОЙ СТРУКТУРЕ

Драголюб М. Спасич
Вооруженные силы Республики Сербия, Генеральный штаб,
Управление по логистике (J-4), г. Белград, Республика Сербия

Резюме:

В данной работе описано численное моделирование ударных повреждений, образовавшихся вследствие удара снаряда по металлической структуре и цели. В работе представлены

результаты экспериментов, испытывающих влияние формы головки снаряда на последствия от удара снаряда о металлическую бронь. Эксперименты проводились на основании ударов снарядов по металлической брони, выполненной из стали и алюминия различной толщины. В ходе эксперимента учитывалось и влияние изменения скорости движения снаряда на последствия от его удара. Для того чтобы эффекты экспериментального моделирования удара выглядели максимально реалистичными, скорость удара снарядов варьировалась от средней до граничной баллистической скорости, при которой осуществлялся пробой преграды. Полученные результаты эксперимента полностью совпали с проведенными реальными действиями на металлические преграды и соответствуют результатам исследований, опубликованых в заграничных изданиях.

Ключевые слова: воздушное судно, авиационные структуры, удар, ударные повреждения, моделирование, снаряд, бронебойный снаряд, пенетратор, прорыв снаряда, проникание, баллистическая защита.

НУМЕРИЧКО МОДЕЛОВАЊЕ УДАРА ПРОЈЕКТИЛА О МЕТАЛНЕ СТРУКТУРЕ

Драгољуб М. Спасић
Војска Србије, Генералштаб, Управа за логистику (J-4), Београд,
Република Србија

Сажетак:

У раду је описано нумеричко моделовање ударних оштећења која настају при удару пројектила о металне структуре. Приказани су и експериментални резултати удара пројектила различитих облика врхова о металне структуре. Експерименти су спроведени ударом пројектила о металне препреке од челика и алуминијума различитих дебљина са променом брзине удара пројектила. Како би ефекти експерименталних симулација удара били што приближнији стварном, брзине удара пројектила су variране, тако да одговарају просечним и граничним брзинама удара пројектила при којима долази до пробијања препреке. Добијени експериментални резултати су се подударили са спроведеним реалним дејством на металне препреке и сличним испитивањима приказаним у страној литератури.